JOURNAL OF PETROLOGY

Journal of Petrology, 2016, Vol. 56, No. 12, 2445–2472
doi: 10.1093/petrology/egv078
Original Article

OXFORD

Dynamics of Magmatic Sulphide Droplets during Transport in Silicate Melts and Implications for Magmatic Sulphide Ore Formation

Jesse C. Robertson*, Stephen J. Barnes and Margaux Le Vaillant

CSIRO Minerals Resources, Australian Resources Research Centre, Perth, WA 6151, Australia

*Corresponding author. Telephone: +618 6436 8572. E-mail: jesse.robertson@csiro.au

Received October 16, 2014; Accepted December 7, 2015

ABSTRACT

The physics and chemistry of ore formation in magmatic sulphide systems are dominantly controlled by the dynamics and kinetics of transported sulphide liquid droplets. We examine the relative importance of chemical dissolution (owing to changes in sulphide concentration at sulphide saturation in the magma) on droplet size, and conclude that the timescales for dissolution (of the order of several days to thousands of years) are much longer than the timescales for dynamic processes (of the order of seconds). We examine dynamic processes that lead to droplet break-up, and delineate the different domains of behaviour that arez encountered over a range of magma flow regimes from stagnant to turbulent, and according to droplet size. Droplets can break up via a variety of mechanisms including deformation and rupture in turbulent flows, and ligament stretching and relaxation in chaotic laminar flows. Droplets larger than a few millimetres in diameter are likely to break up owing purely to the viscous forces acting on them as they settle through stagnant environments. We conclude that droplet break-up, rather than coalescence, is the dominant mechanism for modifying droplet size populations during flow, and that break-up is particularly likely to be prevalent in turbulent komatiite magma and chaotic flow in basaltic magma. The size distributions observed in sulphide blebs and droplets in nature are interpreted as the result of multiple superimposed processes that are active on different portions of the droplet size distribution: growth of sulphide droplets from sulphide-saturated silicate magma and mechanical accumulations of transported assimilated droplets that have undergone break-up during transport. By determining which droplets are stable and which will undergo break-up we show that the presence of large ($>$2 mm) sulphide droplets or blebs in cumulate rocks is an indicator of proximity to a sulphide source or reworked sulphide liquid pool.

Key words: droplet size distributions; droplet break-up; magmatic sulphide; sulphide dynamics; coalescence; chaotic flow; nickel; platinum; basalt; komatiite

INTRODUCTION

The dominant mode of transport of S from the mantle to the crust is within mafic magmas, but the ability of silicate melts to dissolve S is limited. In many natural cases, sulphur is transported predominantly in the form of an immiscible Fe–S–Ni–Cu–O liquid phase. The accumulation of this phase in specific depositional environments is the essential process in the formation of magmatic ore deposits of Ni, Cu and platinum group elements (PGE), some of which, such as those at Sudbury in Canada and Noril'sk–Talnakh in arctic Russia, constitute some of the world's most valuable ore bodies (Naldrett, 2004; Mungall & Naldrett, 2008).

The physical processes by which sulphide liquids interact with and segregate from transporting silicate

melts remain poorly understood, but are crucial not only to understanding the origin of magmatic ore deposits, but also more generally in understanding the geochemical dispersal of highly chalcophile and siderophile elements such as Ni, Cu and the PGE in the crust and mantle. The question of how far magmatic sulphide liquid droplets may be transported in silicate melts is critical to the genetic understanding of (and exploration for) magmatic sulphide ore bodies.

It is widely assumed that the dominant mechanism for transport of sulphide liquid in silicate magmas is in the form of finely dispersed droplets. The observational evidence for this is relatively limited and comes in the form of rare observations of spherical sulphide droplets frozen into chilled margins of intrusions or lava flows (Mathez, 1976; Prichard *et al.*, 2004; Holwell *et al.*, 2012; Patten *et al.*, 2012), and more ambiguously in the presence of dispersed spherical sulphide 'blebs' within silicate crystal cumulates in komatiites (Fig. 1; see also Keele & Nickel, 1974; Lesher, 1983; Dowling *et al.*, 2004; Barnes *et al.*, 2009*b*; Godel *et al.*, 2013) and other associations such as Pechenga and Sudbury (Barnes *et al.*, 2001; Tuchscherer & Spray, 2002). The size distributions of such sulphide liquid blebs and droplets potentially place constraints on the physical processes acting on the droplet suspensions.

The population of droplet sizes during transport in an ore-forming magma is controlled by three main factors, as follows.

1. The mechanism of entrainment. In most magmatic sulphide deposits in the crust, S is generally held to have been externally derived by assimilation of country rock (Keays & Lightfoot, 2010; Ripley & Li, 2013). Where the country rock is S poor, the initial distribution of droplet sizes will be determined largely by the grain size and physical nature of S-bearing minerals in the contaminant; for example, finely disseminated pyrrhotite in the contaminant would lead to fine droplets in the resulting suspension as the contaminant disaggregates (Robertson *et al.*, 2015). Assimilation of sulphide-rich sediment beds, as in the case of ground melting of sulphidic sediments in extrusive komatiite-hosted deposits, would give rise to a more complex distribution of large and small droplets depending upon the dynamics of the process (Lesher & Campbell, 1993). Where the sulphide droplet load is generated purely by nucleation of new droplets, as in the case of a previously droplet-free silicate melt S content exceeding its S content at sulphide liquid saturation (SCSS) as a result of cooling and fractionation, the population distribution is driven entirely by nucleation and growth kinetics (Mungall, 2002; Holzheid, 2010) and would be expected to follow a log–linear size distribution (Godel *et al.*, 2013) similar to the distributions of crystal size typically observed in homogeneously crystallizing igneous rocks (Cashman & Marsh, 1988).
2. The dynamics of the suspension. Lesher & Groves (1986) postulated that the dynamics of sulphide droplet transport would be controlled by an interplay of forces leading to deformation and break-up on the one hand, and coalescence and enlargement on the other. Droplet break-up is favoured where shear rates within the flow are high (steep velocity gradients near flow margins, or turbulence) or where the droplets are large enough to deform under their own buoyancy. Droplet coalescence is favoured where population densities are high, and where droplets are held in contact with one another for long enough to allow drainage of films of host liquid between them. As with break-up, the process is favoured where surface tension forces are relatively low compared with other dynamic forces (i.e. where droplets are large). Experimental and theoretical investigation of the coalescence by de Bremond d'Ars *et al.* (2001) led to the conclusion that coalescence of droplets is unlikely during flow and is largely restricted to the period after accumulation of high concentrations of droplets at a deposition site.
3. Dissolution of sulphide droplets owing to decreasing SCSS with falling pressure during magma ascent. One of the major arguments for the necessity of externally assimilated sulphide to form ore deposits is the negative pressure dependence of SCSS (Mavrogenes & O'Neill, 1999): any sulphide droplets entrained in magma that is sulphide liquid saturated at mantle depths would be expected to dissolve in the host silicate melt on ascent. This has further implications for understanding the geochemistry of highly chalcophile elements in mantle-derived magmas.

This study is concerned largely with the second and third set of processes; that is, the dynamics of droplets in suspensions, and mechanisms and rates of dissolution. Here we consider the balance of the dynamic magma flow forces and capillary (surface tension-related) forces that control sizes of dispersed sulphide liquid droplets within an ore-forming magma, following on from the few previous experimental and theoretical considerations of the topic (Lesher & Groves, 1986; Lesher & Campbell, 1993; de Bremond d'Ars *et al.*, 2001).

We first present data on size distributions of sulphide blebs in cumulate rocks; both from typical disseminated interstitial magmatic sulphide ores such as are commonly found in komatiites and in olivine- and pyroxene-rich cumulates in small intrusions, and from less common but distinctive globular ores. The data are derived from X-ray tomography measurements using high-resolution microtomographic scanning for the finer disseminated ores, and conventional medical tomographic scanning at $\sim$400 μm resolution for the coarse blebby and globular ores. These results provide a frame of reference for consideration of physical processes.

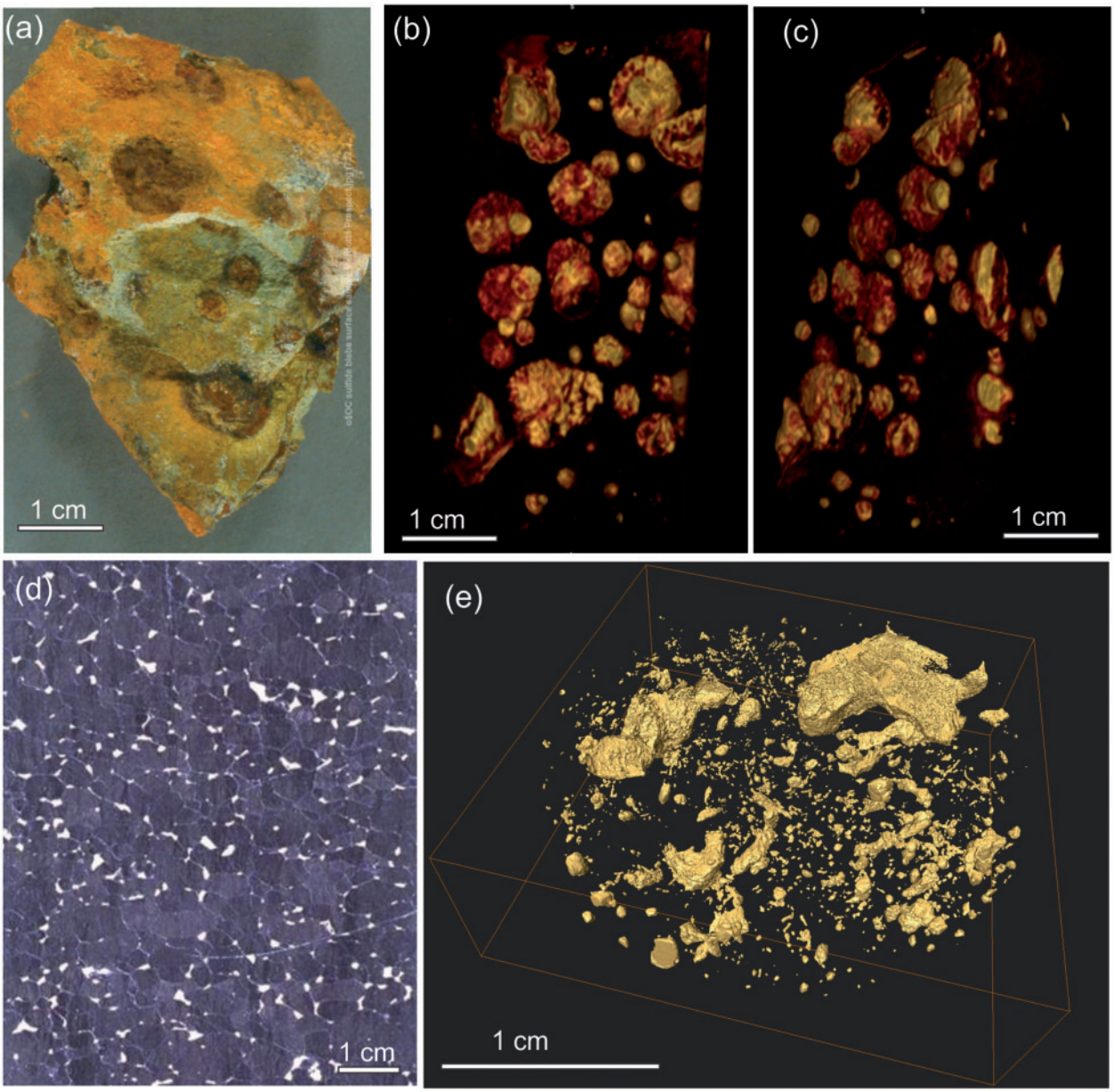

Fig. 1. (a–c) Subspherical sulphide droplets within fine-grained olivine orthocumulate from a komatiite lava flow at Mt Clifford, east Yilgarn Craton, Western Australia. (a) Hand sample showing weathered sulphide droplets (brown); original pyrrhotite–pentlandite pseudomorphed by goethite. (b, c) Orthogonal 3D X-ray tomograms showing the morphology of flattened, originally spherical blebs [(b) in the plane of flattening; (c) normal to the plane]. The greater flattening of the larger droplets, indicating a higher ratio of gravitational to surface tension forces, should be noted. (d, e) Interstitial disseminated composite sulphide (pentlandite–pyrrhotite) blebs within serpentinized adcumulate dunite [in (d), pseudomorphed olivine dark grey, sulphides white] from the Mt Keith nickel deposit, east Yilgarn craton, Western Australia. (e) High-resolution X-ray microtomography image of sulphide blebs (yellow); smaller blebs are generally more equant and spherical than larger ones.

We then examine the kinetic controls on sulphide–magma mass transfer, deriving the relevant timescales for significant mass transfer to take place, and show that (where they are active) flow processes will always dominate thermal processes, which will always dominate chemical processes. To illustrate the problems that 'slow chemistry' raises for traditional geochemical interpretation of these deposits, we consider the effect of changing sulphide liquid solubility (S content at sulphide liquid saturation, or SCSS) on droplet dissolution and calculate the times required to fully dissolve sulphide droplets in an undersaturated magma.

Next we consider the more complex problem of unravelling the physical processes controlling the sizes of sulphide droplets, as they break up and coalesce in both laminar and turbulent magma flows. This complex multiphase flow problem has analogues in a number of physical applications in other fields, from the dynamics of inkjet printers, to the formation of bubbles in waves on the ocean, to the injection of fuel into a piston cavity

in an engine; consequently, the amount of literature on the topic is vast (stretching back to Leonardo da Vinci's study of jet break-up in the Codex Leicester in 1505). Rather than provide a general summary of 500 years of fluid mechanics, we focus on the pieces that are relevant for magma–sulphide suspensions, and use these to determine the likely processes that are acting on droplets of a given size in a given magma. Using these results, we determine the maximum stable droplet size for a given magma, and suggest that droplets larger than these stable sizes indicate proximity to a sulphide source or massive sulphide pool.

SIZES OF SULPHIDE DROPLETS IN NATURE

The sizes of sulphide droplets transported and deposited by magmas can be estimated from observations on quenched sulphide-bearing magmas and from disseminated ores. Quenched magma observations are very rare, whereas several researchers have reported quenched droplets in lavas or small intrusion margins (e.g. Mathez, 1976; Prichard *et al.*, 2004; Holwell *et al.*, 2012); detailed size distributions in two dimensions have been reported only by Patten *et al.* (2012). The droplets reported in mid-ocean ridge basalt (MORB) samples by Patten *et al.* range up to 110 mm in apparent two-dimensional (2D) diameter; 55% of droplets fall between 10 and 20 μm, 38% between 20 and 50 μm, and 7% above 50 μm. Droplets up to 600 μm have been reported in MORB glasses (Czamanske & Moore, 1977). Holwell *et al.* (2012) described globular, mainly spherical sulphide blebs in the margins of mafic macro-dykes in the Tertiary volcanic province in East Greenland. These have characteristic sizes in the 1–2 cm range, but range from 1 mm to 15 cm.

Spherical sulphide droplets are uncommon but widespread in sulphide-bearing komatiitic cumulates (Fig. 1a–c), where typical droplet sizes resemble those in the East Greenland macrodykes (i.e. 1–2 cm), with a long tail of smaller interstitial blebs. In some cases, these droplets are associated with silicate melt 'caps' interpreted as segregation vesicles (Barnes *et al.*, 2009*a*, 2015). Similar features are widespread in the blebby ores of the Noril'sk–Talnakh camp (Spiridonov, 2010). These features are thought to be the result of degassing and bubble formation, with bubbles preferentially associating with the sulphide droplets owing to surface energy effects (Mungall *et al.*, 2015). However, most examples of spherical sulphide droplets show no demonstrable association with vesiculation and show broadly similar size ranges to those that do have that association. They represent the upper range of sulphide liquid droplet sizes in nature.

Primary sulphide droplet sizes have been inferred from 3D microtomographic study of disseminated Ni–Cu–PGE ores in olivine- and pyroxene-rich cumulates (Godel, 2013). Such disseminated ores account for the vast bulk of magmatic sulphide liquid accumulations found in nature, although the much less abundant but much higher grade massive and matrix textured sulphides account for most of what is mined. For example, within the comprehensively studied Agnew–Wiluna komatiite province in Western Australia, based on published resource estimates, in excess of 80% of the sulphide within several billions of tonnes of resources is within the finely disseminated ore type.

A number of assumptions must be made: the distribution of droplet sizes seen in the rocks is not greatly modified by post-cumulus processes and the sample of transported droplets is not significantly biased by the mechanical deposition process. The former assumption was criticized by one of the reviewers of our work, for the case of disseminated sulphides in adcumulate rocks, as found in several of the examples mentioned below, on the grounds that trapped liquid expulsion during adcumulate formation should modify droplet sizes. However, a case has been made in several papers (Barnes *et al.*, 1988; Hill *et al.*, 1995; Godel *et al.*, 2012; Gole *et al.*, 2013) that these rocks formed by *in situ* nucleation and growth of nearly pure olivine–chromite–sulphide adcumulates at the floor of dynamic lava channels, rather than by compaction of a gravitationally formed orthocumulate; hence the original sulphide size population is likely to be preserved.

Data on size distributions in typical disseminated sulphide-bearing cumulates are shown in Fig. 2 for different deposits: Mount Keith, Six Mile and Goliath, all komatiitic dunite-hosted deposits from the Archaean Agnew–Wiluna greenstone belt in Western Australia; Dumont, a komatiitic dunite-hosted deposit in the Abitibi Belt in Quebec; and Kevitsa, an adcumulate wehrlite (olivine-clinopyroxenite)-hosted deposit in Finnish Lapland (see Appendix A for brief deposit descriptions). Sulphide droplet size distributions follow log–linear negative slope distributions, similar to log–linear crystal size distributions (CSDs) observed for silicate crystals in igneous rocks, for samples from a number of different deposits. Godel *et al.* (2013) interpreted such distributions as being mixtures of populations formed by homogeneous nucleation and growth of droplets from the magma and populations of mechanically transported and deposited droplets. The CSD patterns for the five deposits are remarkably similar, differing only in a small proportion of large blebs within the hypothetically transported and deposited population. The near straight-line shapes of the CSD patterns argue against significant mechanical sorting of blebs during deposition, which would tend to produce a strong deficit in the small size fraction.

Droplet morphologies in the much less common globular sulphide ores are shown in Fig. 3. Owing to the much coarser grain sizes, these data were collected on roughly 500 cm^3 sample sizes using a medical computerized tomography (CT) scanner with resolutions of around 400 μm, so the fine end of the size distribution is not resolved (measurement methods are outlined in Appendix B). Data are shown for two samples of sulphide-bearing 'picrodolerite' (actually orthocumulate-textured

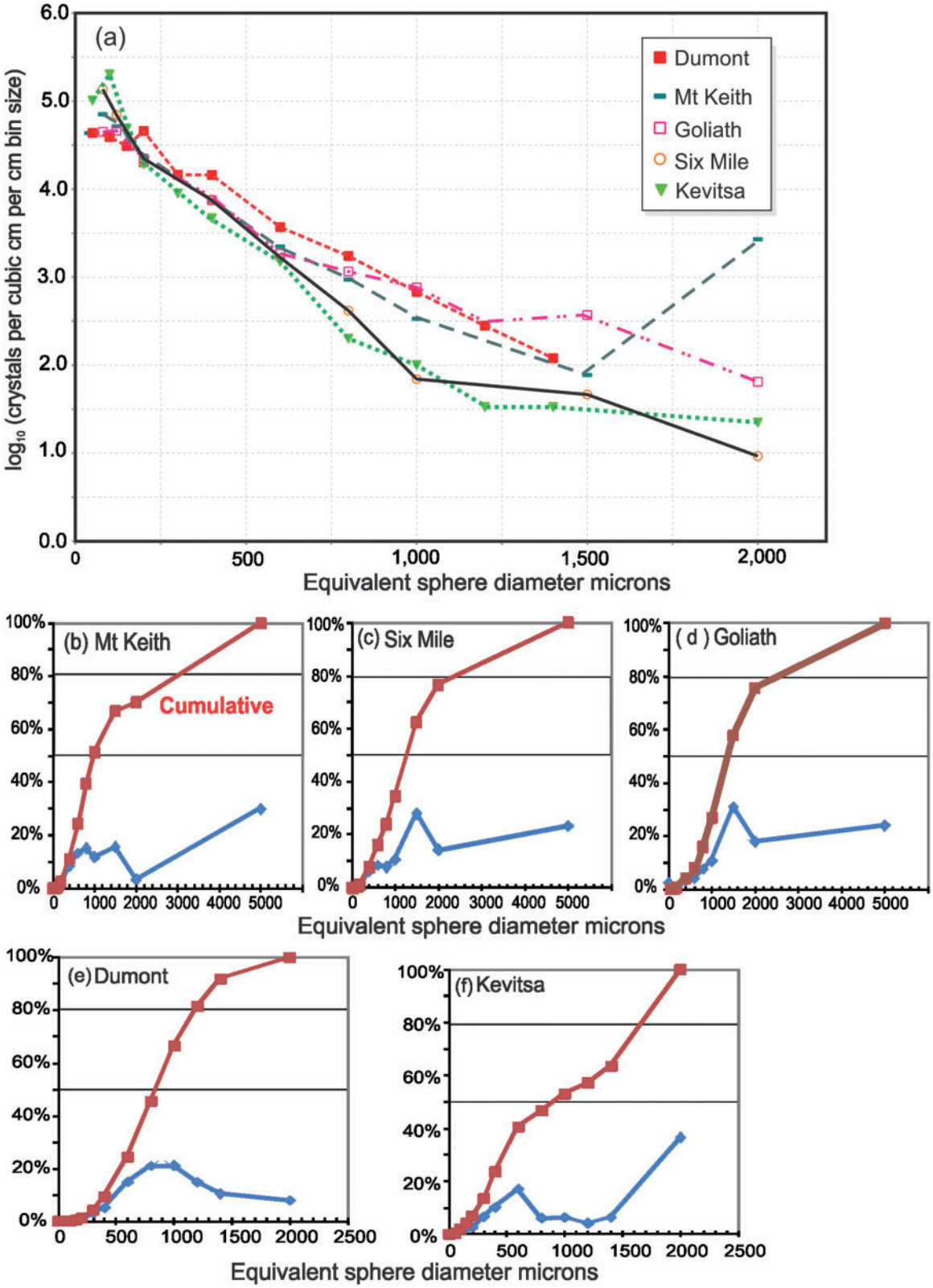

Fig. 2. (a) Particle size distribution plots [equivalent to CSD plots of Marsh (1988)] showing equivalent sphere diameter measurements for sulphide blebs from a number of disseminated ore deposits consisting of 2–5% disseminated sulphide in ultramafic adcumulates; all are from komatiitic dunites except Kevitsa, which is an adcumulate wehrlite (olivine-clinopyroxenite) in a mafic layered intrusion in Finnish Lapland (Mutanen, 1997). (See Appendix A for brief deposit descriptions.) All measurements were made in three dimensions using X-ray microtomography on 2–5 cm^3 samples following the procedure of Godel (2013). The Mount Keith population is composite of five samples. (b–f) Frequency plots weighted by volume showing proportion of total volume of sulphide blebs in the sample falling within the particular bleb size range (blue lines) and cumulative proportion of total sulphide volume falling below the upper limit of bleb sizes (red) (e.g. in the Mt Keith plot, 70% of the total volume of sulphide is in blebs less than 2 mm in equivalent sphere diameter).

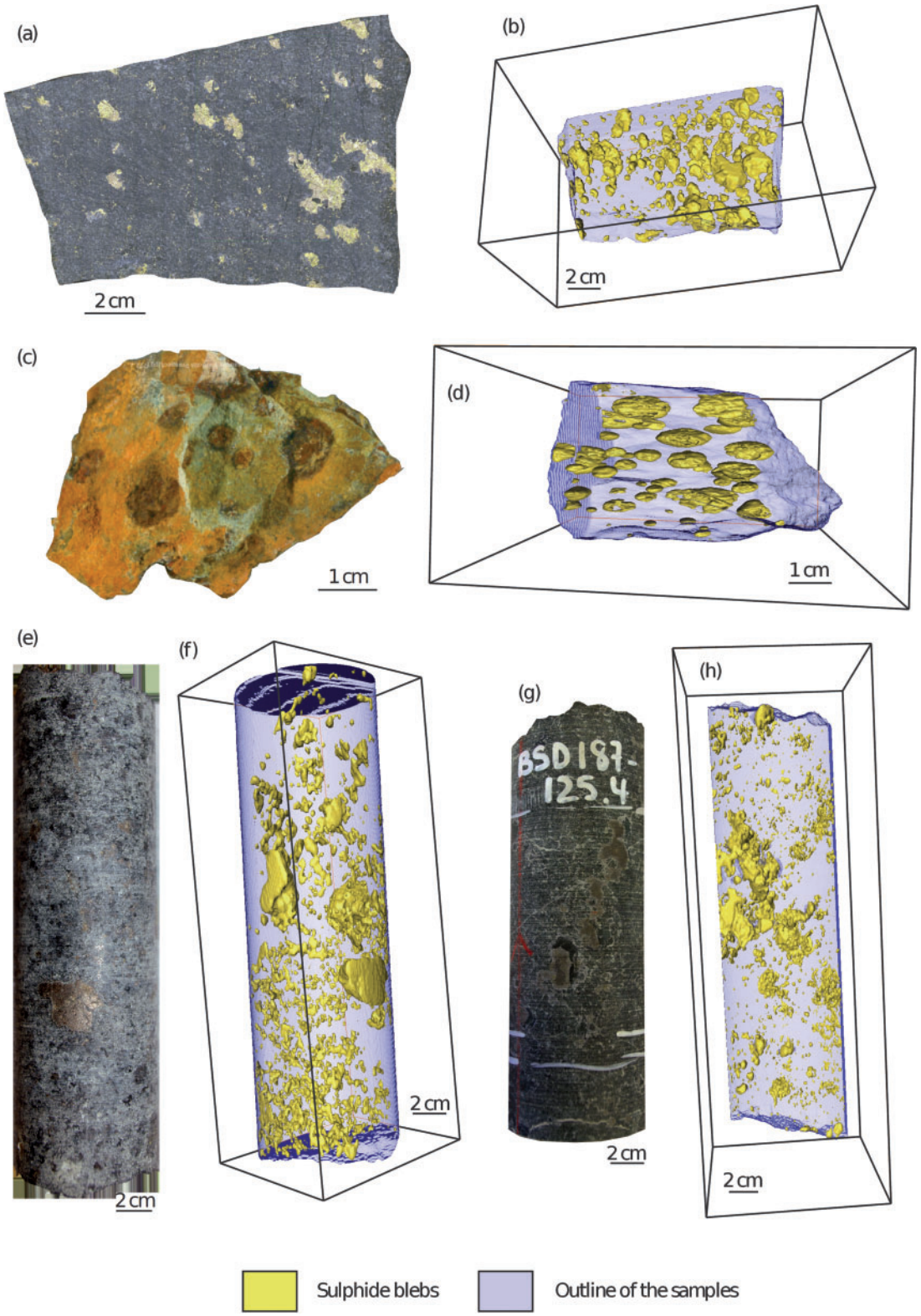

Fig. 3. Core samples and 3D medical scanner images of globular sulphide ores described in the text: (a, b) from a sulphide-bearing 'picrodolerite' at Noril'sk; (c, d) from a coarse-grained olivine orthocumulate in a komatiite flow at Marriotts; (e, f) from Expo–Ungava, a ultramafic dyke-hosted deposit in the South Raglan trend of the Cape Smith Belt, northern Quebec; (g, h) from Black Swan, another coarse-grained orthocumulate komatiite-hosted deposit. The scanning methods are outlined in Appendix A.

olivine gabbro) from the Kharealakh Intrusion in the Noril'sk–Talnakh camp, a sample from the Expo–Ungava ultramafic dyke-hosted deposit in the South Raglan trend of the Cape Smith Belt, northern Quebec (Mungall, 2007), and one sample each from coarse-grained olivine orthocumulates in komatiite flows from Black Swan (Dowling *et al.*, 2004; Barnes *et al.*, 2009b) and the Marriotts deposit (Barnes, 2006).

The Noril'sk samples all show similar straight line log–linear trends up to equivalent sphere diameters of just over 10 mm with a slight excess of larger droplets (Fig. 4). The Expo and Black Swan samples both show kinked distributions, similar to those reported by Godel *et al.* (2013) from Mt Keith and Yakabindie. Significantly, the fine fraction in both Expo and Black Swan falls on a linear trend indistinguishable from that of the cotectic growth population at Mt Keith–Yakabindie, with an excess of larger blebs. The coarser fraction at Black Swan falls on a trend very similar to that defined by the Kharealakh samples. The Marriotts sample is significantly different from all the others, showing an essentially flat distribution with a large deficit of fine blebs less than 2 cm in diameter; consistent with preferential gravitational settling of large droplets. The data on coarser globular ores support the interpretation by Godel *et al.* (2013) that two populations, a cotectic growth population and a coarser transported population, are present in all these examples and in most cases (with rare exceptions) mechanical sorting during deposition does not play a major role.

In summary, the bulk of disseminated sulphide droplets found in diverse magmatic ore systems (and a large proportion of the overall mass of sulphide liquid found in nature) are contained within a size range between about 1 and 5 mm, with a distinct peak between 1 and 2 mm. In the following discussion we refer back to this dataset to provide some constraints on the processes likely to be controlling these distributions.

HOW DROPLET PHYSICS CONTROLS SULPHIDE CHEMISTRY

The key piece of physics underpinning many magmatic processes is the extreme range in characteristic timescales for dynamic, thermal and chemical processes. In general, magma–sulphide chemical interactions are extremely slow compared with thermal interactions, which in turn are extremely slow in comparison with magma flow processes. This can be best seen by comparing the Prandtl, Schmidt and Lewis numbers for magmatic flows, which are dimensionless ratios of these characteristic timescales. A summary of the notation used is given in Table 1.

The Prandtl number is given by

$$\mathrm{Pr} = \frac{\mu_m}{\rho_m \kappa_m} \tag{1}$$

where μ_m, ρ_m and κ_m are the dynamic viscosity, density and thermal diffusivity of the magma respectively. The kinematic viscosity $\nu_m = \mu_m/\rho_m$ can be interpreted as a diffusion coefficient for fluid momentum; high viscosities imply rapid dissipation of fluctuations in fluid momentum. The Prandtl number is the ratio of the momentum dissipation rate to the rate at which thermal diffusion can dissipate fluctuations in heat. A large Prandtl number means that thermal fluctuations are diffused slowly relative to magma flow processes, and therefore thermal equilibrium in magmas will be reached long after dynamic equilibrium. The Earth's mantle (with $\mathrm{Pr} \sim 10^3$) provides an excellent example of high-Pr dynamics: the effects of a change in plate momentum (e.g. a subduction-zone earthquake) are felt at the core–mantle boundary in a matter of minutes to hours, whereas a pulse of heat from the core–mantle boundary will take around 4 billion years to make the same journey via thermal diffusion.

The Schmidt number is the chemical counterpart of the Prandtl number, and is given for chemical species s by

$$\mathrm{Sc_s} = \frac{\mu_m}{\rho_m \kappa_{s,m}} \tag{2}$$

where $\kappa_{s,m}$ is the chemical diffusivity of s in the magma. Similarly to the Prandtl number, a large Schmidt number implies that chemical fluctuations are dissipated slowly relative to magma flow processes. The Lewis number,

$$\mathrm{Le} = \frac{\kappa_m}{\kappa_{s,m}} = \frac{\mathrm{Sc_s}}{\mathrm{Pr}} \tag{3}$$

is the ratio of thermal diffusivity to chemical diffusivity. Large Lewis numbers imply that chemical diffusivity is small relative to thermal diffusivity.

Some example values for Pr and $\mathrm{Sc_s}$ for komatiitic, basaltic and dacitic melts are given in Table 2. For all silicate melt types we have $\mathrm{Sc_s} \gg 1$, $\mathrm{Pr} \gg 1$ and $\mathrm{Le} \gg 1$, which tells us that the time to reach chemical equilibrium via diffusion is much longer (by approximately four orders of magnitude) than the timescale for diffusive thermal transfer, which is in turn much longer (by another six orders of magnitude) than the time taken to reach dynamic equilibrium. To put it more concretely, if a magmatic flow takes 1 s to smooth out a momentum fluctuation over a length scale of 1 m, then it will take nearly a year to diffusively smooth out a similar-sized fluctuation in temperature, and about 300 years to diffusively smooth out a similar-sized fluctuation in chemistry.

Droplet kinetics: how do sulphide and silicate magmas interact chemically?

If chemical processes are so slow, how do sulphide-rich deposits form? Diffusive processes rely on strong gradients to achieve large mass transfer rates: the smaller the diffusivity, the larger the chemical gradient required to achieve the same mass transfer rate. Thus mass transfer requires a dynamic mixing

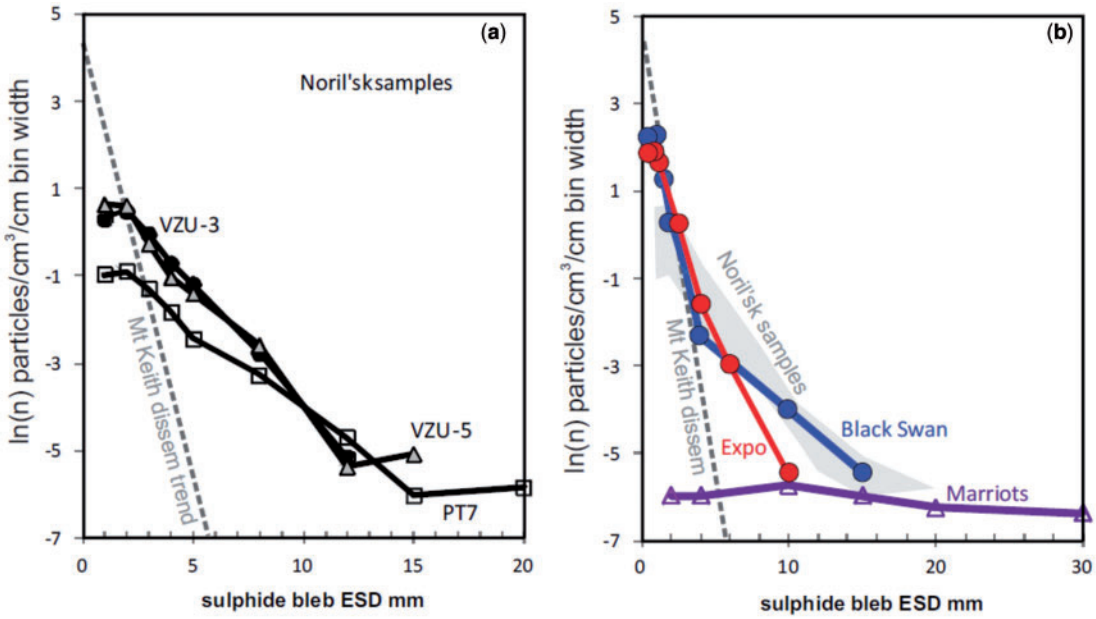

Fig. 4. Droplet size distributions for the globular ores shown in Fig. 3. (a) Data from three Noril'sk samples. All samples have similar droplet size distributions, which deviate from the Mt Keith disseminated nucleation-and-growth controlled trend [from Godel *et al.* (2013), shown for comparison], suggesting that these droplet distributions reflect break-up during sulphide transport. (b) Droplet size distributions for the samples from Expo, Black Swan and Marrriotts. Expo and Black Swan have a fine population fraction with a similar distribution to Mt Keith, and a coarse population with a similar distribution to the Noril'sk samples. In contrast, the sample from Marriotts has a much broader, flatter distribution than the other samples, with a relative deficit in fine fraction droplets, suggesting a high degree of size sorting and/or coalescence during deposition.

Table 1: Summary of notation

Symbol	Definition	Units
a	Droplet radius	m
c	Concentration	kg m^{-3}
C	Coefficient from Hadamard–Rybczynski equation	
ε	Dissipation rate of turbulent kinetic energy	W kg^{-1}
η	Kolmogorov scale	m
f_s	Mass flux of chemical species s	kg m^2 s^{-1}
g	Acceleration owing to gravity	m s^{-2}
$\dot{\gamma}$	Strain rate	s^{-1}
κ	Thermal diffusivity	m^2 s^{-1}
κ_s	Chemical diffusivity for species s	m^2 s^{-1}
μ	Dynamic viscosity	Pa s
ν	Kinematic viscosity	m^2 s^{-1}
σ	Surface tension	N m^{-1}
U	Velocity	m s^{-1}
$\overline{U}$	Mean turbulent velocity	m s^{-1}
Dimensionless parameters		
$\mathrm{Bo} = \frac{\rho g a^2}{\sigma}$	Bond number, ratio of buoyancy forces to surface tension for a droplet of radius a	
$\mathrm{Ca} = \frac{\rho \nu U}{\gamma}$	Capillary number, ratio of viscous stress to surface tension in a flow with characteristic velocity U	
$\mathrm{Pe} = \frac{UL}{\kappa}$	Peclet number, ratio of advection to diffusion. With no subscript this refers to heat advection or diffusion, and with a subscript this refers to chemical species s	
$\mathrm{Pr} = \frac{\mu}{\rho\kappa}$	Prandtl number, ratio of momentum diffusivity to thermal diffusivity	
$\mathrm{Re} = \frac{\rho UL}{\mu}$	Reynolds number, ratio of momentum advection to viscous dissipation	
$\mathrm{Sc_s} = \frac{\mu}{\rho\kappa_s}$	Schmidt number, ratio of chemical advection to chemical diffusion for species s	
$\mathrm{Sh_s} = \frac{af_s}{\kappa_{s,m}(c_{s,m}-c_{s,eq})}$	Sherwood number, ratio of actual mass flux out of a droplet relative to a purely diffusive mass transfer for chemical species s	
$\mathrm{We} = \frac{\rho a U^2}{\sigma}$	Weber number, ratio of inertial stresses to surface tension from external flow. $U^2 \approx E_k(a)$ for a droplet in a turbulent flow	
Superscripts and subscripts		
*	Critical value of a parameter denoting a transition between two dynamic regimes	
m	Property of the host magma	
d	Property of the sulphide droplets	
s	Property of chemical species s	

Table 2: Physical properties assumed for the three magma compositions compared with those of sulphide melts, and calculated Prandtl and Schmidt numbers

Melt type	Density (ρ) (kg m^{-3})	Dynamic viscosity (μ) (Pa s)	Kinematic viscosity (ν) (m^2 s^{-1})
Fe sulphide	4000	2×10^{-2}	5×10^{-6}
Cu sulphide	5200	2×10^{-2}	$3{\cdot}8 \times 10^{-6}$
Komatiite	2800	1	$3{\cdot}5 \times 10^{-4}$
Basalt	2600	100	$3{\cdot}8 \times 10^{-2}$
Dacite	2000	1×10^{4}	5 m^2
Melt type	**Prandtl number Pr**	**Schmidt number Sc**	**Lewis number Le**
Komatiite	350	$2{\cdot}5 \times 10^{6}$	7100
Basalt	38000	$3{\cdot}8 \times 10^{8}$	10000
Dacite	5×10^{6}	5×10^{10}	10000

Data sources are given in Table 3.

Table 3: Physical properties of the sulphide droplets

Property	Symbol	Value	Units
Density	ρ	4000 (Fe-sulphide) 5200 (Cu-sulphide)	kg m^{-3}
Specific heat	c_p	2200	J kg^{-1} °C^{-1}
Thermal diffusivity	κ	6×10^{-6}	m^2 s^{-1}
Thermal conductivity	k	60	W m^{-1} °C^{-1}
Thermal expansion	α	80×10^{-6}	°C^{-1}
Dynamic viscosity	μ	2×10^{-2}	Pa s
Kinematic viscosity	ν	4×10^{-6}	m^2 s^{-1}
Interfacial tension	σ	0·3	N m^{-1}
Heat of fusion	L	$1{\cdot}2 \times 10^{6}$	J kg^{-1}
Melting temperature	T_m	1130 (Fe-sulphide) 1037 (Cu-sulphide)	°C

The physical properties for molten Fe–Cu sulphide are poorly constrained. A collation of values, primarily for FeS from the literature on the properties of the outer core, is given. Sources for these properties are as follows. Sulphide densities and coefficients of thermal expansion are calculated using the model from Kress *et al.* (2008). Specific heat is estimated from data of Deguen *et al.* (2007). Thermal diffusivity and conductivity are estimated using data of Stacey & Anderson (2001). Latent heat of fusion is taken from Anderson (1997). Viscosity is calculated using the model of Terasaki *et al.* (2001) for pure FeS. Interfacial tension is based on a personal communication with James Mungall, and is based on unpublished experimental data.

mechanism to generate large variations over small regions of the flow.

One way to generate strong chemical gradients is through the differential motion between dense sulphide droplets and the host magma. Velocity differences arise because sulphide droplets are approximately twice as dense as the host magma and thus sulphide droplets accelerate at different rates to the host magma. Differential motion is damped out by the viscous drag of the magma.

The best-known example of this is gravitational settling of droplets when there is no flow in the magma. Here a droplet of radius a will settle with a terminal velocity U found from the Hadamard–Rybczynski solution to the Stokes equations:

$$U = \frac{2a^2 g(\rho_d - \rho_m)}{3\mu_m}\left(\frac{1 + \mu_d/\mu_m}{2 + 3\mu_d/\mu_m}\right) \quad (4)$$

(Clift *et al.*, 1978) where ρ and μ are densities and viscosities, respectively, the subscript d denotes a property of the sulphide droplet, and subscript m denotes a property of the host magma, and g is the gravitational acceleration. The full velocity field for this flow is shown in Fig. 5a.

Gravitational settling is not the only way to generate differential motions between droplets and magma—acceleration of the magma around a curved streamline (e.g. around a bend in a magmatic conduit) or direct acceleration in response to a time-varying driving pressure (as in a chaotically stirred flow) will also lead to differential motion with the droplets deviating from the flow paths of the magma (i.e. droplet paths will curve much less than those of the magma). Generally, this means that the size of the velocity difference between the droplets and the magma will be a function of the acceleration history each droplet experiences as it moves through the magma; the governing equations derived by Maxey & Riley (1983) that govern the motion of the droplets explicitly include these terms.

A chemical boundary layer develops at the surface as chemical species are diffused out of the droplet and into the host magma. If the droplet does not move relative to the magma (i.e. for small droplets), this diffusion process leads to a chemical boundary layer that is radially symmetric around the droplet (Fig. 5b). If the droplet is slightly larger or denser so that it settles through the magma, the relative magma flow sweeps the chemical boundary layer around the droplet surface and pulls it off in a long tail (Fig. 5c), which will eventually be mixed through the magma by other dynamic processes or slowly diffused away. As the droplet becomes larger or denser its velocity relative to the magma increases and the chemical boundary layer is stripped away more effectively (Fig. 5d and e). This stripping process does not go on forever: with increasing velocity difference the droplets become increasingly deformed, until the viscous drag exerted by the magma overcomes the droplet surface tension and the droplet breaks up into a set of smaller droplets. We

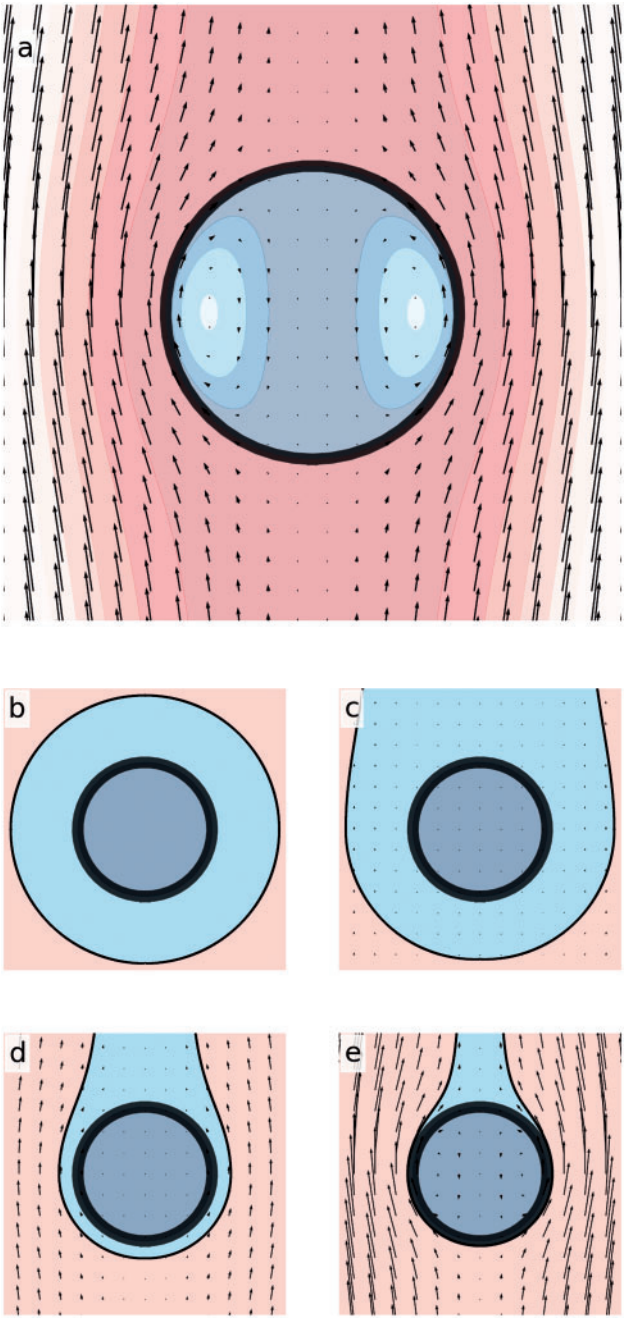

Fig. 5. (a) Structure of the velocity field for viscous flow around a droplet, from a frame of reference moving with the droplet as it falls. The velocity field is given by the Hadamard–Rybzinski solution to the Stokes equations. The shading shows the streamlines of the flow and the arrows show the velocity field. The droplet is shaded in blue and the magma in red. (b–e) Structure of the chemical boundary layer (light blue) separating the droplet (dark blue) from the magma (red), as the droplet Peclet number Pe increases from zero in (b) to a large value in (e). For the magma–sulphide system, an increasing Pe corresponds to either an increase in droplet radius or an increase in density difference from (b) to (e), both of which give a larger terminal velocity.

will assume for now that the droplets are small enough that they remain spherical.

We can combine the effects of both droplet size and density difference into a single parameter known as the Péclet number Pe. This parameter is given for a chemical species s and a droplet of radius a by

$$\mathrm{Pe_s} = \frac{a\Delta U}{\kappa_{s,m}} \tag{5}$$

where $\kappa_{s,m}$ is the diffusivity of species s in the magma and ΔU is the velocity difference between the droplet and the magma. A droplet that is not moving relative to the magma has $\mathrm{Pe} = 0$, whereas larger Péclet numbers denote either higher settling velocities or larger chemical diffusivities, both of which lead to thinner chemical boundary layers and thus more efficient mass transfer between the sulphide and the magma. In principle, each chemical species will have a separate Péclet number and hence a different chemical boundary layer thickness around the same droplet. For simplicity we will assume subsequently that the chemical diffusivities are the same for all chemical species of interest.

The varying thickness of the boundary layer for settling droplets means that the mass transfer varies with position at the droplet surface, with more mass transfer occurring at the upstream end of the droplet. This means that the total mass flux out of the droplet can be found only by integrating this rate over the droplet surface. The integrated mass flux is identified in the literature (e.g. Clift *et al.*, 1978) as a dimensionless ratio of the actual mass flux to the mass flux expected if only diffusion through the melt was acting (i.e. if there was no relative motion between the droplet and the magma). This dimensionless parameter is known as the Sherwood number Sh and is given by

$$\mathrm{Sh_s} = \frac{f_s}{\kappa_{s,m} a (c_{s,m} - c_{s,d})} \tag{6}$$

where f_s is the mass flux of species s between the melt and the droplet, and $c_{s,m} - c_{s,d}$ is the difference in concentration of s between the droplet and the magma. Then Clift *et al.* [1978, equation (3-52), p. 50] gave the result for the Sherwood number for spherical fluid droplets in creeping flow with $\mathrm{Pe_s}$ as

$$\mathrm{Sh_s} \approx 1 + (1 + 0 \cdot 564\mathrm{Pe_s}^{2/3})^{3/4} \tag{7}$$

which is accurate to within 2% for all Péclet numbers. This approximation also recovers two important asymptotic limits—when the Péclet number is large (i.e. the case of large droplets with large terminal velocities whose boundary layers become stripped away) the relationship becomes $\mathrm{Sh} \propto \mathrm{Pe}^{1/2}$. Conversely, when the Péclet number is small (for small droplets, which remain protected by their own chemical boundary layers), mass transfer is via diffusion only, and the Sherwood number is constant: $\mathrm{Sh} = 2$. The variation of Sh with droplet radius is shown in Fig. 6, and indicates that the crossover between large and small droplets occurs at a droplet radius of about 1 mm for komatiites and basalts. This radius corresponds to the 80th to 90th percentile on droplet sizes, and typically about 50% of the total mass of sulphide, as estimated by 3D measurements of

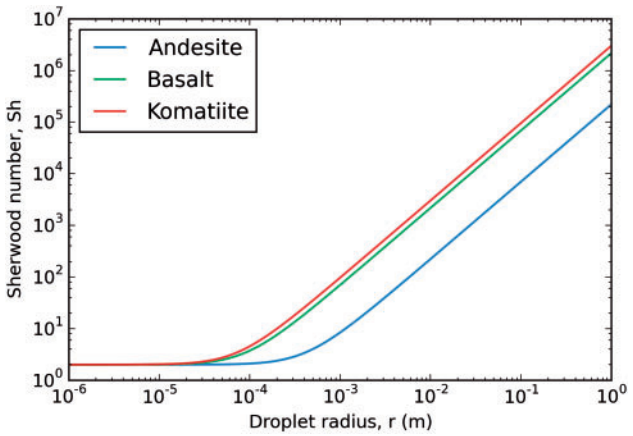

Fig. 6. Variation of Sherwood number with droplet radius for sulphide droplets in komatiitic, basaltic and dacitic magmas.

bleb sizes in natural disseminated ores, as discussed above.

Droplet kinetics, chemistry, and the effect of SCSS on droplet sizes

Sulphide droplets can grow or dissolve in response to changes in the sulphur content of the silicate melt at saturation with sulphide liquid (SCSS). These changes are strongly mediated by pressure and temperature, with additional control by the silicate melt composition and particularly its FeO and Ni contents (Mavrogenes & O'Neill, 1999; Ariskin *et al.*, 2013). Based on the pressure dependence of the SCSS, previous researchers have suggested that magma at depth in the lower crust or upper mantle with an entrained separate sulphide liquid phase will tend to dissolve this sulphide as it ascends to higher levels in the crust, preventing a magmatic deposit from forming. This has been used by a number of researchers (e.g. Lesher & Groves, 1986; Keays & Lightfoot, 2010) to argue that the sulphide in a magmatic ore deposit must be locally derived by melting the wall-rocks. However, here we show that the non-equilibrium chemical dynamics of magma systems (with $Sc \gg 1$) and the kinetics of droplet–magma interaction mean that the pressure dependence of the SCSS does not prevent significant transport of sulphide from deep levels of the crust or even from the upper mantle.

We can use the kinetics considered in the previous section to determine the effect that changing the SCSS of the magma has on the size of a population of sulphide droplets. We do not consider the metal composition of the sulphide explicitly, to focus on the effects of chemical transfer on the droplet size. For a general droplet composition the mass flux for each chemical species will be different owing to the varying diffusivities. However, Mungall (2002) has studied the kinetics of chemical transfer between sulphide and silicate melts in a number of configurations (including both droplets and massive sulphide pools) by explicitly solving the diffusion problem for each species, and showed that the metal compositions in sulphide droplets in a

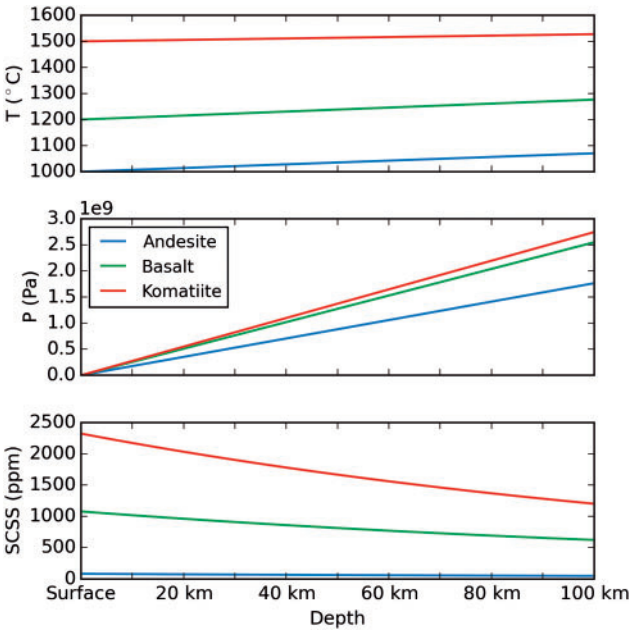

Fig. 7. Profiles of magmastatic pressure (P) and adiabatic temperature (T) vs depth, together with the calculated SCSS profile using the model of Mavrogenes & O'Neill (2002).

number of deposits are controlled by non-equilibrium kinetics. This is simply a consequence of the large-Sc dynamics of the system.

Let us consider a spherical droplet with FeS concentration c_d (the species subscript is omitted for clarity) separated by a chemical boundary layer from a magma containing some concentration of sulphur c_m. The magma immediately adjacent to the droplet's surface is assumed to be in equilibrium with the droplet, so its sulphide content is given by the local value of the SCSS, $c_{eq} = \mathrm{SCSS}(z) = \mathrm{SCSS}[P(z),\ T(z)]$. We have used the SCSS model of Mavrogenes & O'Neill (1999) with an adiabatic temperature profile and magmastatic pressure profile with increasing depth. The SCSS profiles are shown for dacite, basalt and komatiite in Fig. 7. Under these conditions, mass conservation implies that the mass flux of sulphide out of the droplet is balanced by a reduction in the droplet radius:

$$\frac{\mathrm{d}a}{\mathrm{d}t} = \kappa_m \left(\frac{c_m - \mathrm{SCSS}}{\mathrm{SCSS} - c_d} \right) \frac{\mathrm{Sh}}{a} \qquad (8)$$

where $\kappa_m = \kappa_{FeS,m}$ is the diffusivity of FeS in the magma. We assume a value of $\kappa_{FeS,m} = 10^{-10}\ \mathrm{m^2\ s^{-1}}$ as representative of the values given by Mungall (2002). The derivation of this expression follows a similar analysis carried out for sedimenting crystals by Kerr (1994) and an outline is given in Appendix B. To calculate the Sherwood number we use the Hadamard–Rybczynski velocity given in equation (4) as a characteristic velocity difference.

To calculate the radius reduction rate we need to specify the far-field magma composition c_m and a droplet concentration c_d. Here we assume that we have a pure FeS droplet in equilibrium with a magma at

100 km depth, and then consider what happens if we adiabatically decompress the magma by bringing it to the surface. In this case the magma concentration c_m is the SCSS at 100 km depth, whereas $c_d = 1$. Substituting these values into equation (8) gives the dissolution rates results plotted in Fig. 8, which are microns or less per day for basalts and dacites and about 0·1–0·001 mm per day for komatiitic magmas.

By integrating this equation with respect to time we can determine how long the droplets will survive in the sulphide-undersaturated magma. As a worst case, we first consider droplets in komatiite, which would be furthest from equilibrium at the Earth's surface. The change in droplet radius with time for the komatiite case is shown in Fig. 9, with starting droplet radii of 0·5 mm, 1 mm, 5 mm and 1 cm. In the komatiite, the calculations show that an initially millimetre-sized droplet requires about 168 days to fully dissolve, whereas a centimetre-sized droplet will survive for over 900 days. Even droplets smaller than 0·1 mm are capable of surviving for several days. To put this in perspective, at a relatively low magma flow rate of 1 m s^{-1}, droplets could be transported anywhere from tens to thousands of kilometres before dissolving. These survival times suggest that a deposit could still form even after exposure to sulphide-undersaturated magmas, provided the droplets can be separated from the magma quickly (or frozen into place in a lava flow).

As shown in Fig. 9, droplets in basalt or dacite are likely to survive for much longer periods than those in komatiites, because of the lower solubility of sulphide, together with lower diffusion rates and settling velocities giving lower Peclet numbers. Droplets of the size range reported above for MORB (typically less than 100 μm) should be able to survive for anything from a year to several decades within MORB magmas.

To conclude, we note that the kinetics for chalcophile element transfer into the droplets is essentially the same as for sulphide dissolution, with the major difference being the mass transfer direction. Thus, we agree with Mungall (2002) that the chemistry of sulphide droplets preserved in ore deposits is likely to have been kinetically controlled, and to have been substantially out of equilibrium with the transporting magma. This is a significant limitation on the simple application of equilibrium calculations such as the R-factor of Campbell & Naldrett (1979).

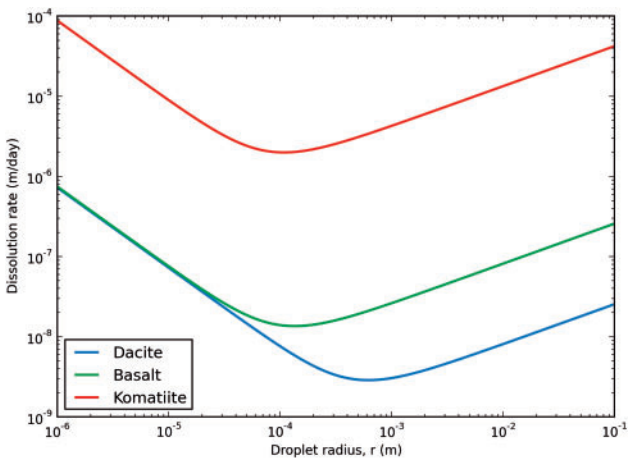

Fig. 8. Dissolution rates for sulphide droplets when brought from 100 km depth to the surface as a function of droplet radius.

PHYSICAL PROCESSES AFFECTING DROPLET SIZES

The previous section has shown that the dominant control on the chemistry of a magmatic sulphide deposit is the size of the droplets during magma–sulphide mixing. However, predicting the droplet sizes for a given magma flow or deposit is difficult, as the droplet size distribution we observe is the result of a complex set of interacting physical flow processes. Although previous researchers have considered only the effect of dissolution or nucleation on size populations (e.g. Mungall, 2002), the analysis above suggests that rapid fluid dynamic processes of break-up and coalescence (acting on the scale of seconds), if they are active, should overwhelm any effects of dissolution (acting on the scale of tens to hundreds of days at best).

Nevertheless, dynamic processes are also tied inherently to droplet size, so different portions of the droplet size distribution can be controlled by different processes at the same time. As a general rule, physical break-up and coalescence processes are most effective on large droplets, whereas small droplets tend to be unaffected. When the dynamic forces in each process are small they can be balanced by the surface tension; when they are large the droplet will become increasingly deformed until it breaks up. Because the size of the surface tension force is related to the curvature of the droplet, smaller droplets have higher surface tensions and can better resist the dynamic forces. This means that we can separate the droplet size population into two categories—small droplets whose sizes are stable, and large droplets, which are unstable. Between these two sub-populations there is a critical droplet size, which is determined by the physical properties of the magma, sulphide and the fluid dynamic forces in question. Our aim in this section is to consider the physical processes separately to determine their critical droplet size and to determine which parts of a droplet population might be controlled by which process.

Dynamic droplet break-up mechanisms

We consider three processes that act to break larger droplets apart into smaller droplets: (1) laminar flows in which droplets are stretched into ligaments that subsequently break up; (2) break-up of droplets via gravitational settling through a quiescent magma; (3) turbulent magma flows in which eddies deform and rupture the droplets. In each section below we outline the theory

giving the critical droplet radius separating stable and unstable droplet sizes for the three processes considered, and calculate some examples for the komatiitic, basaltic and dacitic melt properties given in Table 1.

Ligament-mediated break-up in laminar flows

Under a steady external laminar flow a droplet will deform until the viscous and pressure stresses exerted on the droplet (and which are trying to deform the droplet surface) are balanced by the interfacial tension (which will try to pull the droplet back to a spherical shape). There are two deformation regimes to consider, as follows.

1. At low deformation rates (so that viscous stresses are low) the droplets are kept spherical by the tendency of the interfacial tension to reduce the curvature of the droplet surface (because a sphere is the shape with the least surface curvature for a given volume of fluid). As the viscous forces induced by the external flow increase the droplet takes on an increasingly elongated shape with pointed ends. The length of the deformed droplet is determined by a balance between the increased viscous force and the increased surface tension forces generated by deforming the droplet surface (Clift *et al.*, 1978; Bentley & Leal, 1986).
2. If the deformation increases beyond a critical value the viscous forces overcome the interfacial tension. In this case the droplet will no longer have a stable shape but will instead undergo exponential stretching, drawing out into a fine thread. Once the stretching stops, capillary waves grow on the surface of the ligament and it breaks up—this process is known as the Plateau–Rayleigh instability (Eggers & Villermaux, 2008). Figure 10 illustrates this stretching and break-up process for an initially spherical droplet in a chaotically stirred laminar flow.

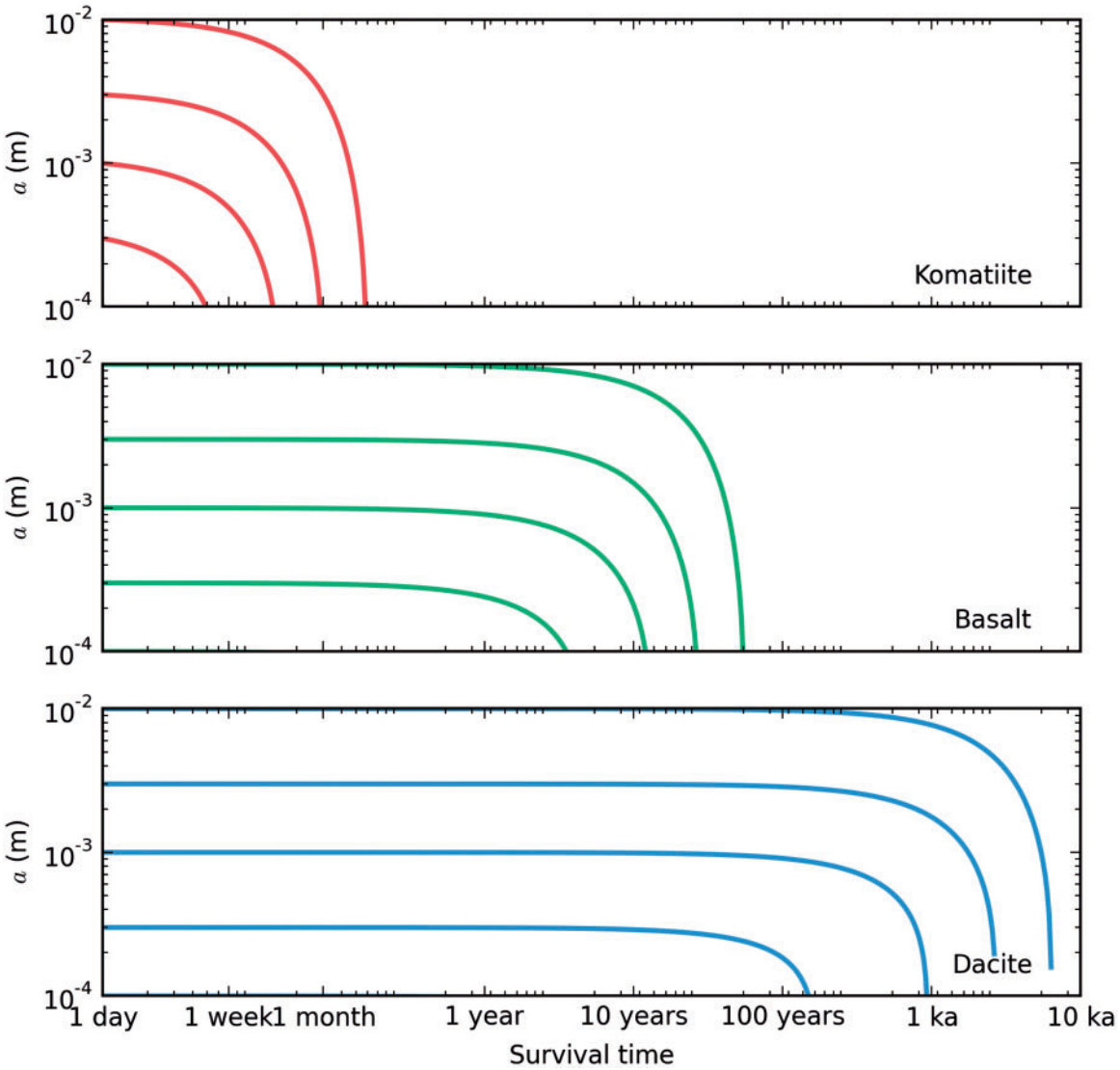

Fig. 9. Change in droplet radius with survival time for sulphide droplets brought from 100 km to the surface by komatiite, basalt and dacite magmas. Model parameters are described in the text. The log scale on the survival time axis should be noted.

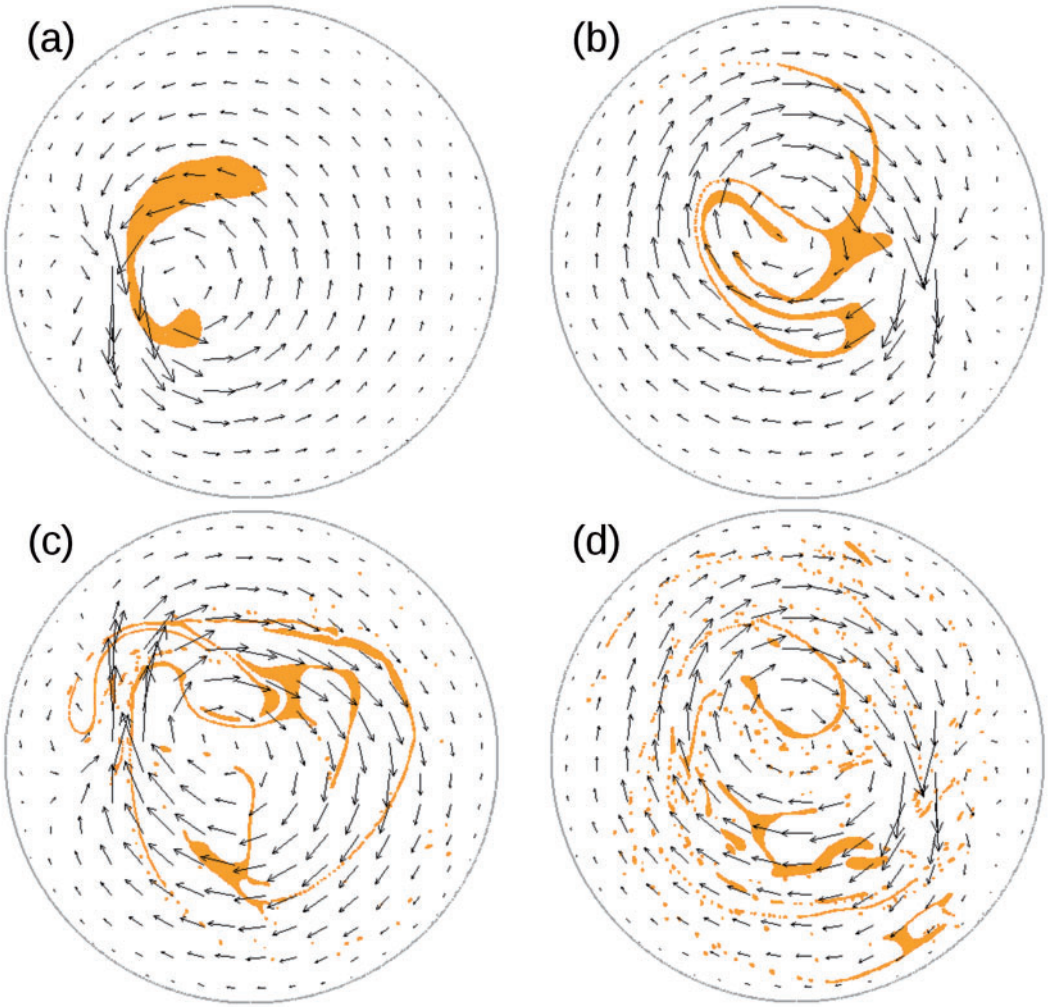

Fig. 10. Stretching and break-up of a high capillary number droplet in a chaotically stirred laminar flow. An initially spherical droplet is stretched by a moving laminar vortex into finer and finer ligaments. Eventually the ligaments undergo break-up via Plateau–Rayleigh instabilities, forming a fine population of daughter droplets (with radii of the same order as the stretched thread), which are small enough to be stable. Each snapshot (a, b, c, d) shows the droplet after 1, 3, 4 and 5 oscillations, respectively, of the stirring vortex. It should be noted that there will be an even finer population of satellite droplets, which form at the same time as the daughter droplets (Khakhar & Ottino, 1986; Tjahjadi & Ottino 1991); these are not resolved by this simulation. (See Appendix C for sim0ulation details and the Supplementary Data for a video version of this figure.)

The location of the transition between these regimes is dependent on the properties of the droplets and the magma, and the style of flow, which determines the size of the viscous shear forces for a given shear rate. As an example of how the flow style affects droplet deformation, spherical shapes typical of low viscous stresses can often be maintained as the shear rate increases if the vorticity of the imposed flow is high. In this case the droplet responds by rotating quickly with the flow (Bentley & Leal, 1986). Consequently, there is little differential motion across the surface of the droplet and the viscous stresses exerted on the droplet by the external flow are small.

To quantify the transition between stable and unstable droplets, we may consider the low-deformation regime in which droplets attain steady shapes in response to the shearing. If the external magma flow generates a shear rate $\dot{\gamma}$ in the vicinity of the droplet, the droplet feels a viscous shear stress of order $\mu_m\dot{\gamma}$ per unit surface area. At steady state this viscous stress is balanced by the surface tension forces; the magnitude of the surface tension force per unit area is approximately σ/a, where σ is the surface tension and a is the radius of an undeformed droplet. This ratio of viscous to interfacial forces acting on a droplet is called the capillary number Ca:

$$\mathrm{Ca} = \frac{a\mu_m\dot{\gamma}}{\sigma}. \quad (9)$$

The two deformation regimes discussed above correspond to low and high values of Ca respectively. In particular, there is a critical value of $\mathrm{Ca} = \mathrm{Ca}^*$ for a flow, which corresponds to a critical droplet radius. Droplets with $\mathrm{Ca} < \mathrm{Ca}^*$ have a steady stable shape,

whereas no steady shape exists for droplets with $Ca > Ca^*$.

In general, the value of Ca* is dependent on the physical properties of both the droplet and the host fluid, and also on the nature of the applied host fluid flow. Bentley & Leal (1986) and Khakhar & Ottino (1986) have carried out experiments and theoretical analysis for the case of relatively low-viscosity droplets and threads deformed in a range of flow configurations and shown that for pure straining flow (where the fluid is stretched in one direction and flattened in the other directions) Ca* is given by

$$Ca^* \approx 0 \cdot 0501 \left(\frac{\mu_d}{\mu_m}\right)^{-2/3} \quad (10)$$

whereas for simple shear (where there are equal amounts of pure strain and rotation) Ca* is given by

$$Ca^* \approx 0 \cdot 148 \left(\frac{\mu_d}{\mu_m}\right)^{-1/6} \quad (11)$$

(the above relationships were given by Khakhar and Ottino (1986, p.279). These critical capillary numbers imply a critical droplet radius,

$$a^*_{cap} = \frac{\sigma Ca^*}{\mu_m \dot{\gamma}} \quad (12)$$

which shows that for a given flow configuration, increasing the deformation $\dot{\gamma}$ or magma viscosity μ_m, or decreasing the surface tension σ will allow smaller droplets to be stretched into ligaments and broken up. Similarly, the critical capillary numbers are much smaller for extensional flow than for simple shear flows, so extensional flows will tend to produce smaller droplets via ligament stretching processes.

Surface tension is still active even after a droplet has been stretched into a ligament. If the forces deforming the droplet are removed, capillary or Plateau–Rayleigh instabilities grow and eventually pinch the ligament into a number of smaller droplets (Eggers & Villermaux, 2003). In general, the low viscosity of the sulphide means that it is stretched almost passively by the magma flow into very fine threads, producing many smaller daughter droplets, which may be fine enough to remain stable, as seen in Fig. 10c and d. The size of the daughter droplets will be similar to the radius of the ligament (although slightly larger as a stretched segment relaxes into a spheroidal bubble); thus, ligaments that are stretched further (and end up thinner) will tend to produce smaller droplets. It should be noted that this process is different from the binary splitting process suggested for solid fragmentation. Whereas break-up in fragmentation occurs by cascade of discrete fracture events, here many daughter droplets are formed at the same time, and it is the ligament stretching (and hence the magma flow) that controls the daughter drop size (Eggers & Villermaux, 2003).

Gravitationally induced droplet break-up

As droplets settle through their host magma under their own weight they experience a drag force from the magma. Small droplets, settling slowly, can balance the viscous drag forces with surface tension. However, large droplets or slugs of sulphide can settle fast enough that density-driven (Rayleigh–Taylor) or shear-driven instabilities at the droplet surface are able to form; if they grow quickly enough they can break the droplet apart.

Although no one has studied the gravitational break-up of sulphide droplets specifically, we can expect that gas bubbles and sulphide droplets may behave similarly, because they both have low viscosity relative to the magma, and both should display similar break-up behaviours. Numerical experiments studying the behaviour of gas bubbles in magmas (Suckale *et al.*, 2010) show the bubbles flattening and forming ring structures, which become gravitationally unstable and break apart into smaller bubbles.

The Rayleigh–Taylor instabilities leading to break-up originate on the lower surface of the droplet (where there is a gravitationally unstable configuration of fluids, with dense sulphide overlying relatively light magma). To cause break-up these instabilities must not be damped by surface tension, or be swept away by the flow around the droplet before they can grow large enough to break the droplet up. The first of these conditions corresponds to a requirement that the droplets be deformable. The relevant dimensionless parameter measuring deformability is known as the Bond number Bo. It is the ratio of the buoyancy of the droplet $(\rho_d - \rho_m)ga$ (where g is the acceleration owing to gravity) to the surface tension σ/a, giving

$$Bo = \frac{(\rho_d - \rho_m)ga^2}{\sigma}. \quad (13)$$

Bubbles with small Bond numbers have a high enough surface tension to remain spherical under their own weight, whereas larger bubbles with high Bond numbers are ‘deformable’. The numerical results of Suckale *et al.* (2010) show that the Bond number needs to be higher than a critical value $Bo^* \approx 100$ for break-up to occur. This critical Bond number implies a critical droplet radius

$$a^*_{Bo} = \left[\frac{Bo * \sigma}{(\rho_d - \rho_m)g}\right]^{1/2} \quad (14)$$

which is about 5 cm for all the magmas considered here.

The second way that droplets can break up is through the growth of shear instabilities at the droplet surface. This will occur when the droplet Reynolds number, given by

$$Re_d = \frac{\rho_m \Delta U a}{\mu_m} \quad (15)$$

becomes large. The numerical experiments of Suckale *et al.* (2010) show that break-up occurs for droplets with $Re_d > \sim 10$, which also implies a critical radius,

$$a^*_{Re} = \left(\frac{\mu_m Re^*_d}{\rho_m C}\right)^{1/3} \quad (16)$$

where C is the coefficient of droplet radius in the Hadamard–Rybczynski equation (i.e. $U = a^2 C$). The critical radius for komatiites is about 7 mm, for basalts about 1·6 cm and for dacites about 8 cm. This implies that shear instabilities are likely to control gravitational break-up of large droplets in komatiites and basalts, whereas Rayleigh–Taylor instabilities control break-up in more viscous magmas such as dacites.

Eddy-induced droplet break-up in turbulent flows

A turbulent flow can be characterized as an interacting cascade of eddies over a range of length scales. Energy is pumped into eddies at the largest scales (for magmas, these eddies might have a similar length scale L to the width of the dyke or flow); these eddies are large enough to be unaffected by the viscosity of the magma. However, the largest eddies transfer inertia to smaller eddy structures, so there is a net energy flux from large to small scales. This energy flux (known as the turbulent energy dissipation rate, ε) generates a cascade of energy, which continues to finer and finer scales, until the energy of the smallest eddies can be dissipated by viscosity as heat.

Droplet break-up within this turbulent eddy field is controlled by the interaction between turbulent inertial stresses from the magma eddies, which act to deform and rupture the sulphide droplets, and the magma-sulphide surface tension, which acts to keep the droplets spherical. Break-up occurs if the turbulent stresses are larger than the surface tension. Figure 11 illustrates a large sulphide droplet breaking up in a turbulent eddy field.

However, only a small subset of eddies in a turbulent flow can induce droplet break-up. We can discard eddies with length scales that are larger than the droplet radius, as the droplet will tend to be carried around in the eddy rather than being broken up. However, the nature of the turbulent energy cascade means that larger eddies have more kinetic energy than smaller eddies, implying that eddies that are much smaller than the droplet will be less likely to cause rupture (because they have less energy) than eddies of the same size as the droplet. This can be seen in Fig. 11b versus Fig. 11d—in Fig. 11b the initial deformation of the droplet induced by the eddy field has a large length scale, whereas in Fig. 11d the finer threads and droplets are affected by smaller-scale eddies. Thus we need consider only the energy in eddies at the same length scale as the droplet.

To make this more precise, we consider the ratio of dynamic forces from the turbulent flow to droplet surface tension, known as the Weber number We. A measure of dynamic force generated by these eddies is given by $\rho_m \overline{U}^2$, where $\overline{U}$ is the mean turbulent velocity fluctuation induced by the eddies at the scale of the droplet. Recalling that the surface tension force for a droplet of radius a is σ/a, the Weber number is defined as

$$We = \frac{a\rho_m \overline{U}^2}{\sigma}. \quad (17)$$

Droplets with We greater than some critical value We* will tend to be broken up. This relationship shows that larger droplets will have higher Weber numbers and are therefore more likely to be broken up. We* can be determined from experiment, with typical values in the range of 1–4 (Hinze, 1955). However, because the Weber number depends on the turbulent velocity $\overline{U}$, we need to know something about the nature of the turbulent flow and the energy cascade across different length scales to evaluate We for different droplets.

The simplest turbulent flow is one in which the probability of finding some fluctuation in velocity is independent of position and time, known as fully developed homogeneous turbulence. These assumptions simplify the analysis as the turbulent dissipation rate ε is then the same at all scales. In this case the energy cascade leads to a specific distribution of energy amongst the different eddy sizes:

$$\overline{U} \approx 2(\varepsilon a)^{2/3} \text{ for } \eta < a < L \quad (18)$$

(Batchelor, 1953). The finest scale at which the dissipation occurs is known as the Kolmogorov scale η, after Kolmogorov (1941*a*, 1941*b*). For a turbulent flow this scale is given by

$$\eta = \left(\frac{\mu_m^3}{\varepsilon \rho_m^3}\right)^{1/4}. \quad (19)$$

The turbulent dissipation rate can be estimated from the rate at which energy is added to the largest eddies (at the scale of the conduit or flow width), so that

$$\varepsilon \approx \frac{\rho_m U L}{\mu_m} \quad (20)$$

where U and L are the velocity and length scales of the large-scale flow (e.g. Campbell & Turner, 1989). For komatiite flows with velocity scales of $U \sim 10$ m s^{-1} and $L \sim 10$–100 m, we obtain $\varepsilon \sim 10$–100 W kg^{-1}, and a Kolmogorov scale of about 1 mm. Given this velocity distribution we find that the critical Weber number We* corresponds to a critical droplet radius a^*_{turb}, given by

$$a^*_{turb} = 2^{-8/5}\left(\frac{\sigma We^*}{\rho_m}\right)^{3/5} \varepsilon^{-2/5}. \quad (21)$$

This critical radius is known in the fluid mechanics literature as the Hinze limit, after Hinze (1955). Droplets with radii below a^*_{turb} are small enough to be unaffected by the turbulent stresses, whereas droplets above a^*_{turb}

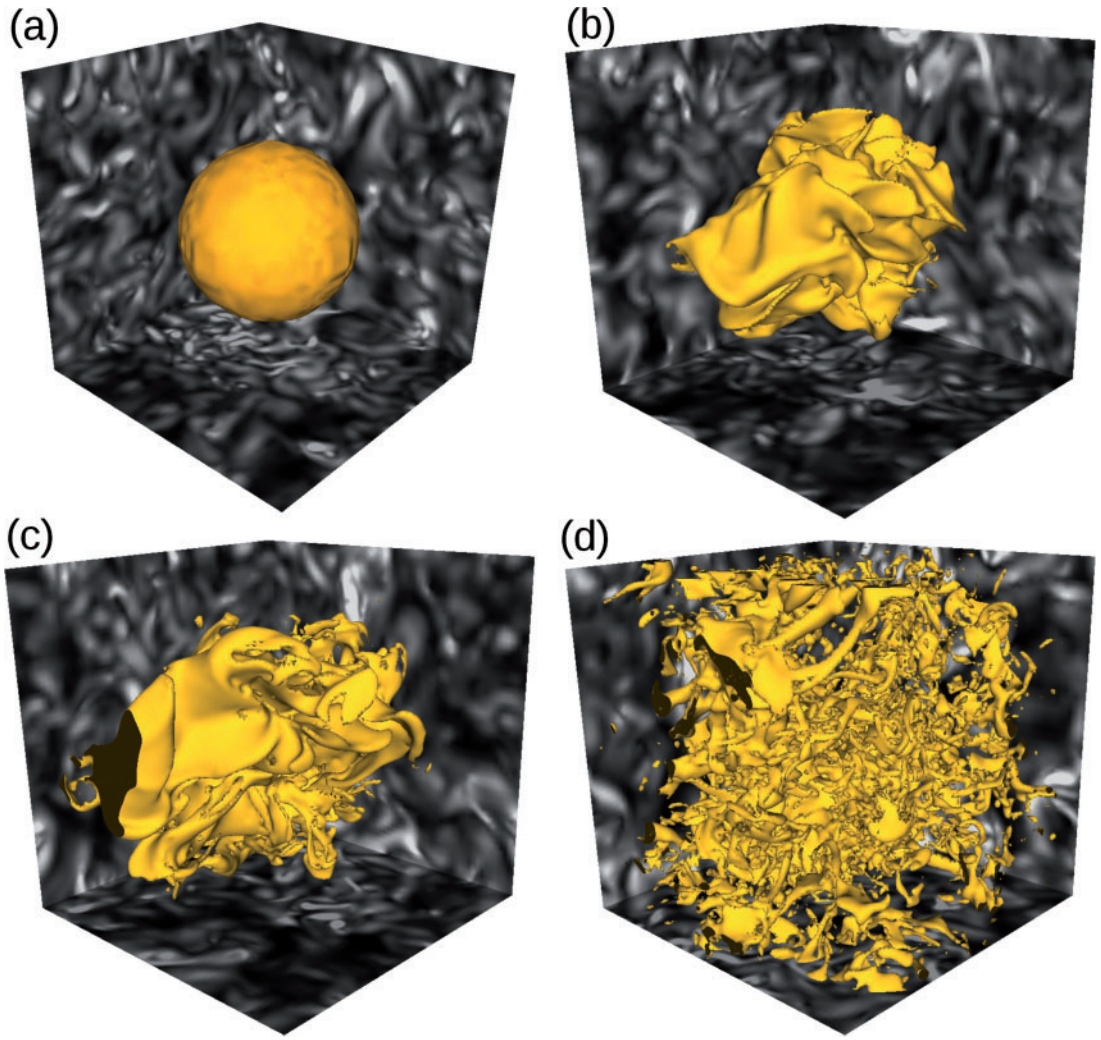

Fig. 11. Fragmentation and break-up of a high Weber number droplet in a turbulent flow. The walls to the box show the field of turbulent vortices, shaded by absolute vorticity. When these vortices collide with the sulphide droplet they pull out ligaments and sheets of sulphide material. It should be noted that the initial deformation is at the scale of the droplet, with finer threads affected by finer vortices as fragmentation continues. The finest filaments will break up via the same Plateau–Rayleigh mechanism as shown in Fig. 10. The size of the domain in Fig. 10 is similar to the scale of the finest vortices in this simulation. (See Appendix C for simulation details and the Supplementary Data for a video version of this figure.)

are more likely to be broken up by turbulent eddies. However, droplets below the Hinze limit in turbulent flows are not necessarily stable; they can still break up via the viscous laminar processes discussed above.

Of the magma types considered here, only komatiites have a low enough viscosity to be fully turbulent (Turner *et al.*, 1986). Estimates of large-scale flow velocities in komatiite flows are up to 10 m s^{-1}, and flow and dyke thicknesses are of the order of 10–20 m. Using these estimates as values for U and L we find that the dissipation rate ε ranges from 10 to 100 m^2 s^{-3}. This means that the Hinze limit radius a^*_{turb} ranges from 1 to 0·1 mm, with the smaller values corresponding to higher values of ε. Referring again to the distribution of droplet sizes observed within komatiite-hosted disseminated ores, and taking the higher end of the Hinze limit range, we estimate that around 80% of droplets in komatiite flows, or about 50% of the total mass of sulphide liquid, fall below the limit; the larger blebs in such settings may have been large enough to be subject to turbulence-driven break-up if the flow was turbulent.

Coalescence

Acting against the processes discussed in the previous section (all of which generate smaller droplet sizes) is droplet coalescence, which creates larger droplets. Although coalescence is observed for bubbles in magmas (Manga & Stone, 1994), it is less well understood for sulphide droplets. Whether coalescence is important in determining the sizes of a population of sulphide droplets depends on two factors: the coalescence time (i.e. the length of time required for two droplets to merge once they are brought into contact), and the interaction frequency (the number of droplet interactions per unit volume per unit time).

The coalescence time is principally determined by the rate at which the intervening film of magma can flow out of the way. For two droplets to coalesce the intervening magma film must thin to the point where it can break so that the two droplets can join. The film thinning rate is controlled by a balance between the magma–sulphide surface tension (which provides the pressure driving the drainage of the magma film between droplets) and the magma viscosity (with larger viscosities requiring longer drainage times; Manga & Stone, 1993). Once the film breaks and the two bubbles join the surface tension pulls back the ruptured film and the droplets will return to a spherical shape over a capillary timescale that scales as $\mu_m a/\sigma$. This timescale is fast: for a komatiite the capillary timescale is $\sim 3 \times 10^{-3}$ s for a millimetre-sized droplet, whereas for a basaltic magma it is about a third of a second. Active shearing assists the drainage of the magma film, and larger, more deformable droplets (with lower surface tensions and lower viscosities) coalesce more readily.

The two droplets have to be held together while these thinning, breaking and withdrawal processes take place. The coupling of two droplets is assisted by the interaction of the flow fields induced by the droplets, and by deformation of the droplets. The relevant dimensionless parameter measuring deformability is the Bond number Bo, defined in equation (14). Experimental studies (Manga & Stone, 1993,1994) have shown that droplets with Bond numbers greater than unity are best able to coalesce, with deformation of the bubbles acting to hold bubble pairs together while the intervening films drain. In all the magmas considered here, sulphide droplets with radii larger than about 5 mm have Bond numbers greater than unity, and should thus be able to coalesce in active flows. Droplets smaller than this will have such high surface tension forces that they will tend not to coalesce.

To study droplet interactions and coalescence in an actively flowing magma conduit, de Bremond d'Ars *et al.* (2001) carried out analogue experiments with droplets of silicone oil in a vertical pipe flow. Those researchers did not observe any coalescence of the droplets within the pipe flow, and film drainage took a long time, even once droplets were allowed to settle at the base of the pipe. Based on these experiments de Bremond d'Ars *et al.* concluded that coalescence does not occur for sulphide droplets during transport. However, this result seems to be inconsistent with observations of coalescence of gas bubbles in basaltic magmas, which have similar Bond numbers and therefore should have similar coalescence characteristics. We suggest that the problem may be the influence of the walls of the pipe flow on droplet–droplet interactions. Droplets may start interacting while they are still several droplet radii away from each other. If they are near a wall that interaction may be inhibited and the wetting and coalescence behaviour described by Manga & Stone (1994) may not occur. This suggests that to approach more closely the conditions in magmatic systems, further experiments are needed on larger populations of droplets to determine adequately the interaction rate. This needs to be in an experiment in which wall effects do not inhibit droplet–droplet interactions. These reservations aside, theoretical considerations are consistent with the experimental observations.

The second control on coalescence, the interaction rate, is possibly more important in active magmatic systems. Higher interaction rates mean more chances that two droplets will remain together and coalesce via the processes discussed above. The relative proportions of sulphide melt and silicate melt [R-factor of Campbell & Naldrett (1979)] involved in the pre-deposition stage of formation of magmatic ores are relatively well constrained, through consideration of mass balance and partitioning of highly chalcophile elements such as the platinum group elements (PGE). Typical magma to sulphide ratios for Ni–Cu-dominated deposits range from tens to low thousands, with typical values for most deposits falling in the hundreds (Campbell & Barnes, 1984). Similarly, proportions of droplets in quenched magmas are typically low (considerably less than 1%). At these proportions the likelihood of particle interactions between sulphide droplets is small.

Very high concentrations of accumulated sulphide liquid, including pools of pure sulphide liquid at the 10 m scale, can be found in ore deposits where they clearly represent the result of mechanical sorting and segregation of sulphide from the original host silicate melt. If segregation occurs quickly enough then an emulsion of sulphide and magma may form, which over time will separate into a separate massive sulphide layer (Zeig & Marsh, 2005). The low volume fractions of sulphide observed in mafic systems suggest that some form of concentration of droplets, either by trapping droplets in a small fraction of the magma flow, or by gravitational settling and congregation at the floor of the conduit, will be required before coalescence can take place.

Combined effects of droplet processes

A combination of all the break-up processes in terms of droplet radius is shown in Fig. 12. The break-up processes in the turbulent flow of komatiitic magma are shown in Fig. 12a. The turbulent dissipation is plotted on the ordinate—larger values mean more turbulent flow and a larger range between the large energy-containing eddies and the Kolmogorov scale where viscous effects are important. Each of the critical radii for the break-up mechanisms considered are plotted and the region of unstable droplet shapes is shaded in the same colour. In regions where multiple break-up mechanisms overlap, the fastest mechanism will generally control the droplet break-up. Droplet size distributions in this flow will show a plateau of small, stable droplets with sizes up to about 0·5 mm, followed by a population of droplets that are liable to be broken up by ligament stretching, up to several millimetres in size. This is then

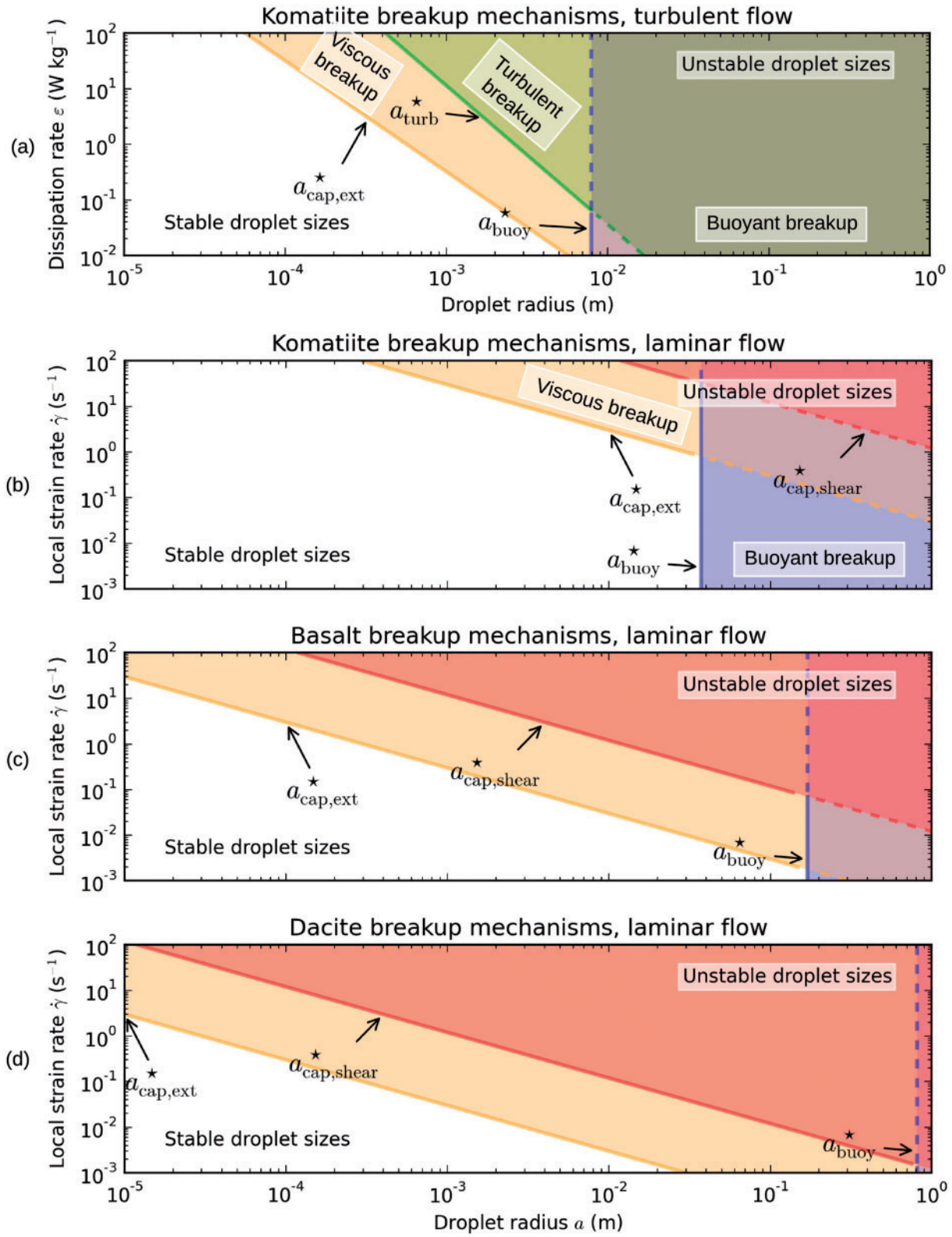

Fig. 12. Droplet break-up mechanisms mapped out for varying magma types and flow conditions, and by droplet radius. Shaded areas denote droplet sizes, which are unstable, with the shading colour corresponding to the mode of break-up. Critical radii bounding these regions are labelled: a^*_{turb} is the critical radius for break-up owing to turbulent eddies, a^*_{buoy} is the critical radius for break-up under buoyant flow, and $a^*_{\mathrm{cap,ext}}$ and $a^*_{\mathrm{cap,shear}}$ are the critical radii for capillary break-up under extensional and shear flows respectively.

followed by droplets that are large enough (i.e. above the Hinze limit) to be affected by the turbulent eddies. Generally the droplet size distribution will fall off much more rapidly than those in the ligament break-up regime. It should be noted that buoyant break-up is important only at very low dissipation rates (i.e. very weak turbulence).

Similar diagrams for laminar flows are shown in Figs 12b–d. Here, local shear rate is plotted on the ordinate, and the diagrams are created for basaltic and dacitic magmas as well as komatiite. Given that these flows are laminar, the Hinze limit is infinitely large and is not shown on these diagrams. We show the two critical capillary radii (where the shear radius, shown in red, is always much larger than the critical radius under extension, shown in orange). The blue box denotes the region of buoyantly unstable droplets, and is much larger for komatiite than for basalt or dacite. Most of these differences are related to the different viscosity of the magma.

Just because a droplet lies within an unstable region of the diagrams in Fig. 12, it does not necessarily follow that it will break up immediately. Droplets must first experience the conditions required to break them up and may be transported for some distance before this occurs. If a hand sample or drill core has many droplets that lie within the unstable size regions, this suggests that they have not been transported very far since remobilization out of a large body of sulphide.

The long timescales associated with sulphide–magma chemical kinetics discussed above suggest that droplets can require a long 'exposure time' in the magma to obtain really high tenors (of a similar timescale to the dissolution survival times shown in Fig. 9). Long exposures are possible if sulphides undergo multiple mobilizations, break-up and depositional cycles. The diagrams in Fig. 12 provide a means of visualizing these cycles: increases in magma flow push droplets upwards, whereas decreases bring them downwards to lower strain and turbulence rates; unstable regions of the plots push droplets to the left, whereas stable regions can push droplets towards larger droplet radii (if they coalesce and form larger droplets) or slowly towards lower radii (if they start to dissolve). Droplets trace out a complex path through these diagrams depending on the local flow conditions in the magma. Dynamic recycling of sulphide through combinations of deposition, gravity-driven backflow and re-entrainment provides the opportunity for droplets to equilibrate efficiently with large volumes of silicate melt, much more efficiently than through processes of simple entrainment and settling, allowing large R-factors and high tenors to be attained.

CONSTRAINTS FROM NATURAL SULPHIDE BLEB SIZE DATA

Interpretation of real datasets (such as those presented in Fig. 2) is difficult; the range of droplet sizes observed in the field is a consequence of a cumulative history of all the processes described above, rather than a snapshot of a population of droplets at a given point in time under a single flow configuration. However, we can use the calculations in the previous sections to infer the likely processes controlling observed droplets of different sizes.

Droplet distributions at Mt Keith

The morphology and size of the sulphide aggregates and associated olivine grains from the Mount Keith deposit were discussed in detail by Godel *et al.* (2013) and summarized above. Sulphide aggregates as imaged in three dimensions by X-ray microtomography (μXCT) are for the most part smaller than the olivines and form disconnected aggregates moulded around the olivine grains. Locally they form interconnected networks with lengths up to five times (but typically two times) the characteristic olivine grain diameters, extending along triple-point channels between the olivines. Barnes *et al.* (2008) and Godel *et al.* (2013) concluded that these aggregates represent original sulphide liquid droplets that had undergone little coalescence since accumulation, and were representative of the original size distribution of sulphide droplets at the time of deposition.

Godel *et al.* (2013) observed straight-line particle size distributions on the droplet size distribution plots (Fig. 2), where the particles are the sulphide aggregates, hereafter referred to as blebs. They further identified two distinct size populations among the blebs: a finer one with a steep CSD slope, and a coarser one with a shallower slope, along with isolated coarse outliers representing larger coalesced blebs. The finer blebs have distinctly lower Pd contents, based on the proxy of measured Pd content in pentlandite, than the coarser population. This led to the conclusion that the smaller population represented a cotectic component of chemically deposited sulphide liquid precipitated from sulphide liquid saturated magma simultaneously with olivine growth, whereas the coarser population represented mechanically transported and deposited droplets that had reacted with larger relative volumes of magma, hence attaining higher PGE contents.

An important question is whether the size of the droplets in the transported fraction was caused by turbulent break-up processes, buoyant break-up, coalescence of smaller droplets or laminar stretching. We begin by assuming that the Mt Keith komatiite magma had similar physical properties to the komatiite considered in our study, and that the largest eddies in the flow had approximate length scales of tens of metres, and velocity scales of tens of metres per second (Turner *et al.*, 1986). This allows us to use the estimate of the turbulent dissipation rate of $\varepsilon \sim 10\,\mathrm{W\,kg^{-1}}$; we find that the Hinze limit for the sulphides at Mt Keith is of the order of 5 mm. Therefore any eddies generated by turbulent flow of the komatiite during emplacement are unlikely to have had a major effect on the size

distribution of most of the observed sulphides. Similarly, calculations of the Bond number suggest that only droplets about 5 mm or larger will be able to coalesce easily. Finally, droplets need to be larger than 7 mm to undergo buoyant break-up, much larger than the droplet sizes observed. We therefore conclude that the observed size distribution of transported sulphides (i.e. those above about 2 mm diameter) is controlled primarily by ligament-mediated viscous break-up processes.

Globular ores, viscous break-up and a possible role for chaotic advection

All of the droplet size populations from the five disseminated deposits represented in Fig. 2 show similar, rather regular log–linear size distributions (between 100 μm and 5 mm). The finer fractions of the size distributions in the coarse blebby ores (Fig. 3) fall on the same distributions, implying a common control with the disseminated ores, whereas the coarser fractions fall on a more shallow power-law distribution. We follow Godel *et al.* (2013) in ascribing the fine fractions as being controlled predominantly by nucleation and growth of newly formed sulphide droplets. The coarser populations, however, show more variance in their distributions and require a different mechanism.

We have shown that a possible mechanism is viscous droplet break-up, similar to that shown in Fig. 10, where the sizes of the daughter droplets are set by the size of the stretched ligament immediately before break-up. Stronger stretching leads to thinner ligaments and smaller daughter droplets. These viscous break-up mechanisms lead to exponentially tailed droplet distributions [Eggers & Villermaux, 2008, their equation (301)] which show up as the log–linear dependences in Fig. 2. However, the fall-off of the distribution is set by the average ligament volume, which is tied inherently to the structure of the flow that is forming the ligament. Is there a way forward to interpret these distributions in terms of the flow dynamics and magma properties if we do not know the flow geometry *a priori*?

One way forward may be to consider the stretching rates in chaotically mixed magma during sulphide transport. Chaotically mixed flows are not turbulent, but rather are time-dependent laminar flows where stretching and folding leads to a fine lamellar structure driving intermingling of fluids (Aref, 1984; Ottino *et al.* (1992)). The role of chaos in magma mixing has been well established by a number of researchers in both volcanic and plutonic settings (Wallace & Bergantz, 2002; Perugini *et al.*, 2005, 2008; De Campos *et al.*, 2008). These observations have been supported by experimental work generating the same mixing morphologies and chemical spatial variability using analogue and natural materials in the laboratory (e.g. Perugini *et al.*, 2002, 2005, 2006).

There are two important features of chaotic systems—first, the lamellar structures exhibit the same properties at different length scales (they are self-similar), and, second, parcels of fluid that started close together exponentially diverge as the flow progresses (particle paths are sensitively dependent on their initial conditions; Turcotte, 1992). It is these features of chaotic flows that make them excellent candidates for mixing sulphide and magma in a laminar way, facilitating chalcophile element transfer into the sulphide and providing a mechanism to attain the R-factors inferred from mass-balance calculations. Numerical studies by Muzzio *et al.* (1991) found that the self-similar structure of chaotic flows leads to a time-invariant statistical distribution of stretching flow elements. Using these distributions it should be possible to tie the average ligament size to the average stretching rate, thus obtaining a droplet size distribution, from which mass transfer rates could be obtained and thus a link between flow dynamics and deposit chemistry. However, the dataset we have in hand includes only the droplet distribution, not the magma properties or the stretching distribution, and we require one of these to be able to infer the other. More work across a range of deposits with differing magma types is required before we can unravel this complex piece of physics.

SULPHIDE LIQUID SOLUBILITY AND ORE GENESIS

Many published discussions of magmatic sulphide ore genesis emphasize the importance of the sulphide liquid solubility, strictly expressed as the S content at sulphide liquid saturation, or SCSS. The importance of this quantity in understanding ore-forming processes needs to be understood from the standpoint of droplet physics. There are in effect three distinct paths to sulphide liquid formation from a mantle-derived mafic or ultramafic magma, as described below.

Attainment of sulphide saturation during fractional crystallization or mixing without external S addition

In this first scenario, previously sulphide-undersaturated magmas may evolve towards sulphide liquid saturation by processes completely independent of addition of external components; simple fractional crystallization and/or saturation of oxidized magmas with magnetite (Jenner *et al.*, 2010) are capable of achieving this end. This is the most likely explanation for disseminated sulphide layers associated with highly evolved cumulates in layered intrusions such as the Platinova Reef of the Skaergaard intrusion (Andersen *et al.*, 1998) along with other examples (Prendergast, 2000; Maier *et al.*, 2003). In such cases, the sulphide liquid droplets so formed are characteristically extremely enriched in PGE as a result of equilibration with hundreds of thousands of times their own volume of magma (Campbell *et al.*, 1983), and maximum droplet sizes are typically of the order of tens to hundreds of microns (Godel *et al.*, 2014). Droplet sizes would be expected to follow

growth-controlled distributions. The evolution of SCSS with changing magma composition is clearly vital to this process; decrease in SCSS owing to addition of external S without SiO_2 (Li & Ripley, 2009) may contribute in some circumstances. However, droplet populations generated by this process will be heavily weighted towards small, low Bond number droplets that are resistant to coalescence. Highly unusual circumstances of extremely efficient particle entrapment and coalescence would be required to generate large volumes of sulphide-rich ore by this mechanism.

Dissolution of external sulphide by a highly sulphide-undersaturated magma

In this case, sulphide minerals are added to the magma by disaggregation and melting of incorporated xenoliths, and this component may dissolve in initially sulphide-undersaturated magma rather than forming droplets. With subsequent cooling and crystallization, the silicate magma then evolves towards higher S content and lower SCSS, and eventually becomes S-saturated, at which point new droplets form as in the first scenario. This process will be enhanced where assimilation adds enough SiO_2 to affect the SCSS trajectory with cooling (Li & Ripley, 2009). However, the rate of dissolution is very slow, being driven by chemical diffusion, relative to the rate of melting, controlled by thermal diffusion, which is three orders of magnitude faster (Robertson *et al.*, 2015). As noted in the previous discussion, droplets of the order of a millimetre in size would be expected to survive dissolution for periods of months in a typically S-undersaturated basaltic magma, and high proportions of xenomelt (see below) would be expected to survive on this timescale (Fig. 9). The situation of complete dissolution of sulphide xenomelts is therefore probably rather rare. It may be largely restricted to komatiites, where the silicate magma may well start with S contents many hundreds of parts per million below SCSS, and temperatures are high enough and viscosities low enough to facilitate very rapid xenolith melting. This combination of circumstances is required to explain deposits such as those at Mt Keith, where there is unambiguous isotopic evidence for assimilated S (Bekker *et al.*, 2009; Fiorentini *et al.*, 2012) but sulphide droplet populations contain a large cotectic component (Godel *et al.*, 2013).

Direct assimilation and melting of sulphide-bearing xenoliths

In this circumstance, the addition of abundant sulphidic material to the melt results in the formation of a sulphide 'xenomelt', a term introduced by Lesher & Burnham (2001) to denote sulphide melt derived by direct melting of externally derived solid sulphide minerals. Here, the droplet size distribution is controlled initially by the grain size of the sulphide component in the xenolith population, and subsequently modified by break-up. This mechanism is likely to be the major mechanism for the formation of most large Ni–Cu–PGE sulphide-rich deposits. We have argued that kinetic processes dominate over chemical equilibrium in natural silicate–sulphide emulsions. Hence in the case where external sulphide is added to a magma as a result of assimilation of sulphide-bearing xenoliths (Robertson *et al.*, 2015), the presence and degree of equilibration of sulphide liquid droplets in the melt will be determined by a wide range of factors: the nature of the sulphide fraction of the assimilated material, the rate of melting of this component, and the rate of stirring by chaotic mixing processes within the entraining flow and the consequent rate of break-up of the droplets so formed. Dissolution of this sulphide liquid into previously undersaturated silicate magma is only one of these factors. In the case of a basaltic melt, where the SCSS value is only a few hundred parts per million, it is likely to be a relatively minor factor. This is very different from the case where sulphide liquid is forming as result of nucleation and growth of new droplets from a sulphide-saturated melt, where droplets form with growth-controlled particle size distributions, as seen in the fine fraction of typical disseminated ores. This scenario will give rise to droplet size distribution dominated by break-up-driven distributions mixed with a growth-related component.

CONCLUSIONS

In this study we have examined the fundamental role of droplet physics in the formation of magmatic sulphide deposits, as follows.

1. By considering droplet kinetics in response to changes in sulphide concentration at sulphide saturation in the magma, we have shown that dissolution rates (occurring over timescales of days in komatiite to hundreds of years in basalt to thousands of years in dacite) are many orders of magnitude slower than dynamic flow processes controlling droplet break-up (which occur over timescales of seconds).
2. Efficient chemical transfer between sulphide and magma requires sulphide droplets of millimetre size or larger—droplets with radii smaller than this never escape their own chemical boundary layers, which restrict chemical transfer to relatively slow diffusive processes. A further implication of the importance of kinetics on reaction efficiency concerns chalcophile element depletion in the associated silicate magmas. Magmas carrying fine populations of sulphide droplets are unlikely to undergo extensive PGE depletion even where the sulphide proportion is high enough to generate strong depletion at equilibrium. Many published models of the tenors of magmatic sulphide ores require prior extraction of sulphide liquid in very finely calibrated proportions to account for order-of-magnitude PGE depletions in inferred parent magmas (e.g. Lightfoot *et al.*, 2012; Song *et al.*, 2012). The analysis presented here, in agreement

with the conclusions of Mungall (2002), suggests that the degree of depletion of silicate melt in highly chalcophile elements is more likely to be controlled by magma dynamics and boundary layer kinetics than by simple equilibrium processes. Magma–sulphide equilibrium is likely in slow, high-temperature, static processes such as mantle partial melting, but not in dynamic settings such as during assimilation, entrainment and transport. This explains the relative rarity of extremely PGE depleted magmas, even in proximity to genetically associated ore deposits (Fiorentini *et al.*, 2010).

3. Because chemical processes in magmatic systems are so slow, the fluid dynamics during emplacement is by far the most dominant control on the large end of droplet size distributions. Droplets can break up by three mechanisms: (a) ligament-mediated viscous break-up, in which droplets are first stretched into ligaments and allowed to relax and break up into daughter droplets; (b) gravitationally driven break-up, in which the flow associated with buoyant settling drives Rayleigh–Taylor instabilities, which eventually break up the droplet; (c) eddy-induced turbulent break-up, in which the inertia of turbulent eddies in the magma breaks up the droplets.
4. Ligament-mediated break-up is likely to be the most important within the coarser part of the range of typical observed droplet sizes and for the expected range of behaviours of natural magma flow regimes. Ligament-mediated break-up leads to exponential-tailed droplet size distributions, which potentially carry information about stretching rates and the nature of chaotic structures within the flow, but are greatly complicated by superimposed effects such as mixing of growth and break-up populations, and mechanical sorting during deposition.
5. Coalescence of droplets is likely to be important only for droplets with radii larger than a few millimetres, above the limit where one or other of the break-up mechanisms is likely to be dominant, and is hence unlikely during flow transport. We concur with previous experimental results predicting that coalescence should take place only under stagnant conditions. However, more experimental work is needed to test the theory for sulphide–magma systems.
6. Based on data taken from μXCT scans of magmatic ores, we have shown that most of the transported droplets would have been too small to be affected by turbulence in a host komatiite, or by buoyancy-driven break-up, but that chaotic viscous break-up was a factor in controlling droplet sizes during transport. The characteristic log–linear particle size distributions observed in all deposits studied so far within the size fraction less than about 2 mm diameter could be due to either homogeneous nucleation–growth processes or chaotic viscous break-up, or most probably both. Further data on deposits associated with different magma types are required to assess this further.
7. The importance of controls on SCSS has been overstated in the literature on Ni–Cu–PGE sulphide ore genesis. In the case of sulphide-rich Ni–Cu-dominant magmatic sulphide systems with an external sulphide source, the initial state of sulphide saturation of the silicate magma may well be largely irrelevant. Dynamic processes within the flow completely overwhelm the far slower processes controlled by chemical diffusion. Far more important factors are the fluid dynamic environment governing the extent of thermal interaction between magma and country rock and the availability of country rock sulphide along a crustal magma flow network (Barnes *et al.*, 2015).

Considering application to exploration for magmatic sulphide ore deposits, these conclusions suggest that a shift in focus is required: away from the presence of local wall-rock sulphide sources as a targeting tool, and towards a better understanding of trapping and depositional processes, both in conduit-hosted deposits and in lava flow environments. Attention should be paid to factors such as size distributions of sulphide droplets, and the magnitude and scale of local tenor fluctuations. The presence of large ($>$2 mm) sulphide droplets in cumulate rocks implies proximity to a sulphide source and limited transport distance; extended transport should result in break-up of droplets down to the sub-millimetre size fraction. Further, the presence of high-PGE large droplets implies proximity to a reworked magmatic sulphide ore pool within a dynamic conduit system. New techniques such as μXCT, which reveals the three-dimensional details of the droplets making up a deposit, coupled with *in situ* techniques such as laser ablation to measure PGE tenors at the droplet scale, combined with a sound understanding of the relevant fluid dynamics will be crucial to developing a step change in our understanding of magmatic sulphide ore deposits and mineral systems.

ACKNOWLEDGEMENTS

The authors would like to acknowledge the authors of the scientific Python stack and thank them for making their code free and open source. We thank Mike Lesher and Guy Metcalfe for stimulating discussions on the importance of droplet transport in magmatic sulphide ore formation. Bruce Marsh, Nick Arndt and Marian Holness provided extremely helpful reviews that greatly improved the final paper.

FUNDING

The authors were supported by funding from the CSIRO office of the Chief Executive Science Fund.

SUPPLEMENTARY DATA

Supplementary data for this paper are available at *Journal of Petrology* online.

REFERENCES

Andersen, J. C. O., Rasmussen, H., Nielsen, T. F. D. & Ronsbo, J. G. (1998). The Triple Group and the Platinova gold and palladium reefs in the Skaergaard Intrusion—stratigraphic and petrographic relations. *Economic Geology* **93**, 488–509.

Anderson, O. L. (1997). The Grüneisen parameter for iron at outer core conditions and the resulting conductive heat and power in the core. *Physics of the Earth and Planetary Interiors* **109**(3-4), 179–197.

Aref, H. (1984). Stirring by chaotic advection. *Journal of Fluid Mechanics* **143**, 1–21.

Ariskin, A. A., Danyushevsky, L. V., Bychkov, K. A., McNeill, A. W., Barmina, G. S. & Nikolaev, G. S. (2013). Modeling solubility of Fe–Ni sulphides in basaltic magmas: the effect of Ni in the melt. *Economic Geology* **108**, 1983–2003.

Arnold, V. I. (1965). Sur la topologie des écoulements stationnaires des fluides parfaits. *Comptes Rendus de l'Académie des Sciences* **261**, 17–20.

Barnes, S. J. (2006). Komatiite-hosted nickel sulphide deposits: geology, geochemistry, and genesis. Nickel deposits of the Yilgarn Craton: geology, geochemistry, and geophysics applied to exploration. In: Barnes, S. J. (ed.) *Society of Economic Geologists, Special Publication* **13**, 51–118.

Barnes, S. J., Hill, R. E. T. & Gole, M. J. (1988). The Perseverance ultramafic complex, Western Australia: product of a komatiite lava river. *Journal of Petrology* **29**, 305–331.

Barnes, S.-J., Melezhik, V. A. & Sokolov, S. V. (2001). The composition and mode of formation of the Pechenga nickel deposits, Kola Peninsula, northwestern Russia. *Canadian Mineralogist* **39**, 447–471.

Barnes, S. J., Fiorentini, M. L., Austin, P., Gessner, K., Hough, R. & Squelch, A. (2008). Three-dimensional morphology of magmatic sulphides sheds light on ore formation and sulphide melt migration. *Geology* **36**, 655–658.

Barnes, S. J., Makkonen, H. V., Dowling, S. E., Hill, R. E. T. & Peltonen, P. (2009a). The 1·88 Ga Kotalahti and Vammala Nickel Belts, Finland: geochemistry of the mafic and ultramafic metavolcanic rocks. *Bulletin of the Geological Society of Finland* **81**, 103–141.

Barnes, S. J., Wells, M. A. & Verrall, M. (2009b). Effects of Magmatic Processes, Serpentinization, and Talc-Carbonate Alteration on Sulfide Mineralogy and Ore Textures in the Black Swan Disseminated Nickel Sulfide Deposit, Yilgarn Craton. *Economic Geology* **104**, 539–562.

Barnes, S. J., Fiorentini, M. L., Duuring, P., Grguric, B. A. & Perring, C. S. (2011). The Perseverance and Mount Keith Ni deposits of the Agnew–Wiluna Belt, Yilgarn Craton, Western Australia. *Reviews in Economic Geology* **17**, 51–88.

Barnes, S. J., Cruden, A. R., Arndt, N. T. & Saumur, B. M. (2015). The mineral system approach applied to magmatic Ni–Cu–PGE sulphide deposits. *Ore Geology Reviews* Available online 18 June 2015, ISSN 0169-1368, http://dx.doi.org/10.1016/j.oregeorev.2015.06.012, (http://www.sciencedirect.com/science/article/pii/S0169136815001663).

Batchelor, G. K. (1953). *The Theory of Homogeneous Turbulence*. Cambridge University Press.

Bekker, A., Barley, M. E., Fiorentini, M. L., Rouxel, O. J., Rumble, D. & Beresford, S. W. (2009). Atmospheric sulfur in Archean komatiite-hosted nickel deposits. *Science* **326**, 1086–1089.

Bentley, B. J. & Leal, L. G. (1986). An experimental investigation of drop deformation and break-up in steady, two-dimensional linear flows. *Journal of Fluid Mechanics* **167**, 241–283.

Campbell, I. H. & Barnes, S. J. (1984). A model for the geochemistry of the platinum group elements in magmatic sulphide deposits. *Canadian Mineralogist* **22**, 151–160.

Campbell, I. H. & Naldrett, A. J. (1979). The influence of silicate:sulphide ratios on the geochemistry of magmatic sulphides. *Economic Geology* **74**, 1503–1506.

Campbell, I. H. & Turner, J. S. (1989). Fountains in magma chambers. *Journal of Petrology* **30**, 885–923.

Campbell, I. H., Naldrett, A. J. & Barnes, S. J. (1983). A model for the origin of the platinum-rich sulphide horizons in the Bushveld and Stillwater Complexes. *Journal of Petrology* **24**, 133–165.

Cashman, K. V. & Marsh, B. D. (1988). Crystal size distribution (CSD) in rocks and the kinetics and dynamics of crystallization II: Makaopuhi lava lake. *Contributions to Mineralogy and Petrology* **99**, 292–305.

Clift, R., Grace, J. R. & Weber, M. E. (1978). *Bubbles, Drops and Particles*. Academic Press.

Czamanske, G. K. & Moore, J. G. (1977). Composition and phase chemistry of sulphide globules in basalt in the Mid-Atlantic Ridge rift valley near 37°N lat. *Geological Society of America Bulletin* **88**, 587–599.

Czamanske, G. K., Zen'ko, K. E., Fedorenko, V., Calk, L. C., Budahn, J. R., Bullock, J. H. J., Fries, T. L., King, B. S. & Siems, D. F. (1995). Petrographic and geochemical characterization of ore-bearing intrusions of the Noril'sk Type, Siberia; with discussion of their origin. *Resource Geology, Special Issue* **18**, 1–48.

de Bremond d'Ars, J., Arndt, N. T. & Hallot, E. (2001). Analog experimental insights into the formation of magmatic sulphide deposits. *Earth and Planetary Science Letters* **186**, 371–381.

De Campos, C. P., Dingwell, D. B., Perugini, D., Civetta, L. & Fehr, T. K. (2008). Heterogeneities in magma chambers: insight from the behaviour of major and minor elements during mixing experiments with natural alkaline melts. *Chemical Geology* **256**, 131–145.

Deguen, R., Alboussiere T. & Brito, D. (2007). On the existence and structure of a much at the inner core boundary of the Earth. *Physics of the Earth and Planetary Interiors* **164**(1-2), 36–49.

Dombre, T., Frisch, U., Greene, J. M., Hénon, M., Mehr, A. & Soward, A. (1986). Chaotic streamlines in the ABC flows. *Journal of Fluid Mechanics* **167**, 353–391.

Dowling, S. E., Barnes, S. J., Hill, R. E. T. & Hicks, J. (2004). Komatiites and nickel sulphide ores of the Black Swan area, Yilgarn Craton, Western Australia. 2. Geology and genesis of the ore bodies. *Mineralium Deposita* **39**, 707–728.

Duke, J. M. (1986). The Dumont nickel deposit: a genetic model for disseminated magmatic sulphide deposits of komatiitic affinity. In: Gallacher, M. J., Ixer, R. A., Neary, C. R. & Prichard, H. M. (eds) *Metallogeny of Basic and Ultrabasic Rocks*. Institute of Mining and Metallurgy, pp. 151–160.

Eggers, J. & Villermaux, E. (2008). Physics of liquid jets. *Reports on progress in physics* **71**(3).

Fiorentini, M. L., Barnes, S. J., Lesher, C. M., Heggie, G. J., Keays, R. R. & Burnham, O. M. (2010). Platinum-group element geochemistry of mineralized and non-mineralized komatiites and basalts. *Economic Geology* **105**, 795–823.

Fiorentini, M. L., Beresford, S. W., Barley, M. E., Duuring, P., Bekker, A., Rosengren, N., Cas, R. & Hronsky, J. (2012). District to camp controls on the genesis of komatiite-hosted nickel sulphide deposits, Agnew–Wiluna greenstone belt, Western Australia: insights from the multiple sulfur isotopes. *Economic Geology* **107**, 781–796.

Fuster, D. (2013). An energy preserving formulation for the simulation of multiphase turbulent flows. *Journal of Computational Physics* **235**, 114–128.

Godel, B. (2013). High-resolution X-ray computed tomography and its application to ore deposits: from data acquisition to quantitative three-dimensional measurements with case

studies from Ni–Cu–PGE deposits. *Economic Geology* **108**, 2005–2019.

Godel, B., Barnes, S. J. & Barnes, S.-J. (2013). Deposition mechanisms of magmatic sulphide liquids: evidence from high-resolution X-ray computed tomography and trace element chemistry of komatiite-hosted disseminated sulphides. *Journal of Petrology* **54**, 1455–1481.

Godel, B., Gonzalez-Alvarez, I., Barnes, S.-J., Parker, P., Day, J. (2012). Sulfides and sulfarsenides from the rosie nickel prospect, Duketon Greenstone. *Economic Geology* **107**, 275–294.

Godel, B., Rudashevsky, N. S., Nielsen, T. F. D., Barnes, S. J. & Rudashevsky, V. N. (2014). New constraints on the origin of the Skaergaard Intrusion Cu–Pd–Au mineralization: Insights from high-resolution X-ray computed tomography. *Lithos* **190–191**, 27–36, http://dx.doi.org/10.1016/j.lithos.2013.11.019.

Gole, M. J., Robertson, J. & Barnes, S. J. (2013). Extrusive origin and structural modification of the komatiitic Mount Keith Ultramafic Unit. *Economic Geology* **108**, 1731–1752.

Grguric, B. A., Rosengren, N. M., Fletcher, C. M. & Hronsky, J. M. A. (2006). Type 2 deposits: geology, mineralogy and processing of the Mount Keith and Yakabindie ore bodies, Western Australia. Nickel deposits of the Yilgarn Craton: geology, geochemistry, and geophysics applied to exploration. In: Barnes, S. J. (ed.) *Society of Economic Geologists, Special Publication* **13**, 119–138.

Hill, R. E. T., Barnes, S. J., Gole, M. J. & Dowling, S. E. (1995). The volcanology of komatiites as deduced from field relationships in the Norseman–Wiluna greenstone belt, Western Australia. *Lithos* **34**, 159–188.

Hinze, J. O. (1955). Fundamentals of the hydrodynamic mechanism of splitting in dispersion processes. *AIChE Journal* **1**, 289–295.

Holwell, D. A., Abraham-James, T., Keays, R. R. & Boyce, A. J. (2012). The nature and genesis of marginal Cu–PGE–Au sulphide mineralisation in Paleogene macrodykes of the Kangerlussuaq region, East Greenland. *Mineralium Deposita* **47**, 3–21.

Holzheid, A. (2010). Separation of sulphide melt droplets in sulfur saturated silicate liquids. *Chemical Geology* **274**, 127–135.

Jenner, F. E., O'Neill, H. S. C., Arculus, R. J. & Mavrogenes, J. A. (2010). The magnetite crisis in the evolution of arc-related magmas and the initial concentration of Au, Ag and Cu. *Journal of Petrology* **51**, 2445–2464.

Keays, R. R. & Lightfoot. (2010). Crustal sulfur is required to form magmatic Ni–Cu sulphide deposits; evidence from chalcophile element signatures of Siberian and Deccan Trap basalts. *Mineralium Deposita* **45**, 241–257.

Keele, R. A. & Nickel, E. H. (1974). The geology of a primary millerite-bearing sulphide assemblage and supergene alteration at the Otter Shoot, Kambalda, Western Australia. *Economic Geology* **69**, 1102–1117.

Kerr, R. C. (1994). Dissolving driven by vigorous compositional convection. *Journal of Fluid Mechanics* **280**, 287–302.

Khakhar, D. V. & Ottino, J. M. (1986). Deformation and break-up of slender drops in linear flows. *Journal of Fluid Mechanics* **166**, 265–285.

Kolmogorov, A. N. (1941a). Dissipation of energy under locally isotropic turbulence. *Proceedings of the Russian Academy of Sciences* **301**, 16–18.

Kolmogorov, A. N. (1941b). The local structure of turbulence in an incompressible fluid with very large Reynolds number. *Proceedings of the Russian Academy of Sciences* **309**, 301–305.

Kress, V., Greene, L. E., Ortiz, M. D. & Mioduszewski, L. (2008). Thermochemistry of sulfide liquids IV: density measurements and the thermodynamics of O-S-Fe-Ni-Cu liquids at low to moderate pressures. *Contributions to Mineralogy and Petrology* **156**, 785–797.

Lesher, C. M. (1983). *Localisation and genesis of komatiite-associated Fe–Ni–Cu sulphide mineralization of Kambalda, Western Australia*. PhD thesis University of Western Australia, 318 pp.

Lesher, C. M. & Burnham, O. M. (2001). Multicomponent elemental and isotopic mixing in Ni–Cu–(PGE) ores at Kambalda, Western Australia. *Canadian Mineralogist* **39**, 421–446.

Lesher, C. M. & Campbell, I. H. (1993). Geochemical and fluid dynamic modelling of compositional variations in Archean komatiite-hosted nickel sulphide ores in Western Australia. *Economic Geology* **88**, 804–816.

Lesher, C. M. & Groves, D. I. (1986). Controls on the formation of komatiite-associated nickel–copper sulphide deposits. In: Friedrich, G. H. (ed.) *Geology and Metallogeny of Copper Deposits*. Springer, pp. 63–90.

Li, C. & Ripley, E. M. (2009). Sulfur contents at sulphide–liquid or anhydrite saturation in silicate melts: empirical equations and example applications. *Economic Geology* **104**, 405–412.

Lightfoot, P. C. & Zotov, I. A. (2014). Geological relationships between the intrusions, country rocks and Ni–Cu–PGE sulphides of the Kharealakh Intrusion, Noril'sk region: Implications for the role of sulphide differentiation and metasomatism in their genesis. *Northwestern Geology* **47**, 1–35.

Lightfoot, P. C., Keays, R. R., Evans-Lamswood, D. & Wheeler, R. (2012). S saturation history of Nain plutonic suite mafic intrusions; origin of the Voisey's Bay Ni–Cu–Co sulphide deposit, Labrador, Canada. *Mineralium Deposita* **47**, 23–50.

Maier, W. D., Barnes, S.-J., Gartz, V. & Andrews, G. (2003). Pt–Pd reefs in magnetitites of the Stella layered intrusion, South Africa: A world of new exploration opportunities for platinum group elements. *Geology* **31**, 885–888.

Manga, M. & Stone, H. A. (1993). Buoyancy-driven interactions between two deformable viscous drops. *Journal of Fluid Mechanics* **256**, 647–683.

Manga, M. & Stone, H. A. (1994). Interactions between bubbles in magmas and lavas: effects of bubble deformation. *Journal of Volcanology and Geothermal Research* **62**, 267–279.

Marsh, B. D. (1988). On the interpretation of crystal size distributions in magmatic systems. *Journal of Petrology* **39**, 553–599.

Mathez, E. A. (1976). Sulfur solubility and magmatic sulphides in submarine basalt glass. *Journal of Geophysical Research* **81**, 4269–4276.

Mavrogenes, J. A. & O'Neill, H. S. C. (1999). The relative effects of pressure, temperature and oxygen fugacity on the solubility of sulphide in mafic magmas. *Geochimica et Cosmochimica Acta* **63**, 1173–1180.

Maxey, M. R. & Riley, J. J. (1983). Equation of motion for a small rigid sphere in a nonuniform flow. *Physics of Fluids* **26**, 883–889.

Mungall, J. E. (2002). Kinetic controls on the partitioning of trace elements between silicate and sulphide liquids. *Journal of Petrology* **43**, 749–768.

Mungall, J. E. (2007). Crustal contamination of picritic magmas during transport through dikes: the Expo Intrusive Suite, Cape Smith Fold Belt, New Quebec. *Journal of Petrology* **48**, 1021–1039.

Mungall, J. E. & Naldrett, A. J. (2008). Ore deposits of the platinum-group elements. *Elements* **4**, 253–258.

Mungall, J. E., Brenan, J. M., Godel, B., Barnes, S. J. & Gaillard, F. (2015). Transport of metals and sulphur in magmas by flotation of sulphide melt on vapour bubbles. *Nature Geoscience* **8**, 216–219.

Mutanen, T. (1997). *Geology and ore petrology of the Akanvaara and Koitelainen mafic layered intrusions and the Keivitsa–Satovaaa layered complex, northern Finland. Bulletin of the Geological Survey of Finland* **395**.

Mutanen, T. & Huhma, H. (2001). U–Pb geochronology of the Koitelainen, Akanvaara and Keivitsa mafic layered intrusions and related rocks. In: Vaasjoki, M. (ed.) *Radiometric age determinations from Finnish Lapland and their bearing on the timing of Precambrian volcano-sedimentary sequences. Geological Survey of Finland, Special Paper* **33**, 229–246.

Muzzio, F. J., Swanson, P. D. & Ottino, J. M. (1992). Mixing distributions produced by multiplicative stretching in chaotic flows. *International Journal of Bifurcation and Chaos* **2**, 37–50.

Naldrett, A. J. (2004). *Magmatic Sulphide Deposits: Geology, Geochemistry and Exploration*. Springer, 727 pp.

O'Neill, H., St, C. & Mavrogenes, J. A. (2002). The Sulfide Capacity and the Sulfur Content at Sulfide Saturation of Silicate Melts at 1400°C and 1 bar. *Journal of Petrology* **43**, 1049–1087.

Ottino, J. M., Muzzio, F. J., Tjahjadi, M., Franjione, J. G., Jana, S. C. & Kusch, H. A. (1992). Chaos, symmetry, and self-similarity: exploiting order and disorder in mixing processes. *Science* **257**, 754–760.

Patten, C., Barnes, S.-J. & Mathez, E. A. (2012). Textural variations in MORB sulphide droplets due to differences in crystallization history. *Canadian Mineralogist* **50**, 675–692.

Perugini, D., Poli, G. & Gatta, G. (2002). Analysis and simulation of magma mixing processes in 3D. *Lithos* **65**, 313–330.

Perugini, D., Poli, G. & Valentini, L. (2005). Strange attractors in plagioclase oscillatory zoning: petrological implications. *Contributions to Mineralogy and Petrology* **149**, 482–497.

Perugini, D., Petrelli, M. & Poli, G. (2006). Diffusive fractionation of trace elements by chaotic mixing of magmas. *Earth and Planetary Science Letters* **243**, 669–680.

Perugini, D., De Campos, C. P., Dingwell, D. B., Petrelli, M. & Poli, G. (2008). Trace element mobility during magma mixing: preliminary experimental results. *Chemical Geology* **256**, 146–157.

Popinet, S. (2003). Gerris: a tree-based adaptive solver for the incompressible Euler equations in complex geometries. *Journal of Computational Physics* **1902**, 572–600.

Prendergast, M. D. (2000). Layering and precious metals mineralization in the Rincon del Tigre Complex, eastern Bolivia. *Economic Geology* **95**, 113–130.

Prichard, H. M., Hutchinson, D. & Fisher, P. C. (2004). Petrology and crystallization history of multiphase sulphide droplets in a mafic dike from Uruguay: implications for the origin of Cu–Ni–PGE sulphide deposits. *Economic Geology and the Bulletin of the Society of Economic Geologists* **99**, 365–376.

Ripley, E. M. & Li, C. (2013). Sulphide saturation in mafic magmas; is external sulfur required for magmatic Ni–Cu–(PGE) ore genesis?. *Economic Geology and the Bulletin of the Society of Economic Geologists* **108**, 45–58.

Robertson, J. C., Ripley, E. M., Barnes, S. J. & Li, C. (2015). Sulfur liberation from country rocks and incorporation in mafic magmas. *Economic Geology* **110**, 1111–1123.

Song, X. Y., Danyushevsky, L. V., Keays, R. R., Chen, L.-M. & Wang, Y.-S. (2012). Structural, lithological, and geochemical constraints on the dynamic magma plumbing system of the Jinchuan Ni–Cu sulphide deposit, NW China. *Mineralium Deposita* **47**, 277–297.

Spiridonov, E. M. (2010). Ore–magmatic systems at Noril'sl ore field. *Geologiya i Geophyzika* **51**, 1356–1378 (in Russian).

Stacey, F. D. & Anderson, O. L. (2001). Electrical and thermal conductivities of Fe-Ni-Si alloy under core conditions. *Physics of the Earth and Planetary Interiors* **124**, 153–162.

Suckale, J., Hager, B. H., Elkins-Tanton, L. T. & Nave, J.-C. (2010). It takes three to tango: 2. Bubble dynamics in basaltic volcanoes and ramifications for modelling normal Strombolian activity. *Journal of Geophysical Research* **115**, B07410.

Terasaki, H., Kato, T., Urakawa, S., Funakoshi, K., Suzuki, A., Okada, T., Maeda, M., Sato, J., Kubo, T. & Kasai, S. (2001). The effect of temperature, pressure, and sulfur content on viscosity of the Fe -FeS melt. *Earth and Planetary Science Letters* **190**(1-2), 93–101.

Tjahjadi, M. & Ottino, J. M. (1991). Stretching and break-up of droplets in chaotic flows. *Journal of Fluid Mechanics* **232**, 191–219.

Tuchscherer, M. G. & Spray, J. G. (2002). Geology, mineralization and emplacement of the Foy Offset Dike, Sudbury Impact Structure. *Economic Geology* **97**, 1377–1307.

Turcotte, D. L. (1992). *Fractals and Chaos in Geology and Geophysics*. Cambridge University Press.

Turner, J. S., Huppert, H. E. & Sparks, R. S. J. (1986). Komatiites II. Experimental and theoretical investigations of post-emplacement cooling and crystallization. *Journal of Petrology* **27**, 397–439.

Wallace, G. & Bergantz, G. (2002). Wavelet-based correlation (WBC) of crystal populations and magma mixing. *Earth and Planetary Science Letters* **202**, 133–145.

Yang, S.-H., Maier, W. D., Hanski, E. J., Lappalainen, M., Santaguida, F. & Maatta, S. (2013). Origin of ultra-nickeliferous olivine in the Kevitsa Ni–Cu–PGE-mineralized intrusion, northern Finland. *Contributions to Mineralogy and Petrology* **166**, 81–95.

Zeig, M. J. & Marsh, B. D. (2005). Origin of ultra-nickeliferous olivine in the Kevitsa Ni–Cu–PGE-mineralized intrusion, northern Finland. *Geological Society of America Bulletin* **117**(11-12), 1427–1450.

APPENDIX A: DESCRIPTIONS OF LOCALITIES MENTIONED IN THE TEXT

The droplet size data in Fig. 2 were collected from samples of a number of different disseminated Ni and Ni–Cu–PGE sulphide deposits. In this appendix we provide a brief geological description of these deposits.

The Mount Keith, Goliath and Six Mile deposits are all large (>1 million tonnes contained Ni, typical grades around 0·6% Ni), low-grade, disseminated sulphide deposits located within the Archaean Agnew–Wiluna greenstone belt in the north–central Yilgarn Craton of Australia, ~400 km NNW of Kalgoorlie. The greenstone belt and its deposits has been described in detail by Barnes (2006), Barnes *et al.* (2011) and Fiorentini *et al.* (2012).

Mount Keith

The Mount Keith deposit occurs within the Mount Keith Ultramafic Complex, a lenticular body, *c.* 700 m thick by 2 km wide, of coarse-grained dunite formed as olivine–sulphide cumulates from a very high Mg komatiite parent magma (Barnes *et al.*, 2011). The body formed

by accretion of cumulates within a large open komatiite flow channel, probably a deeply entrenched lava flow (Hill *et al.*, 1995; Gole *et al.*, 2013). It contains a large, low-tonnage, centrally disposed ore deposit comprising volumetrically minor but high-tenor disseminated Fe–Ni sulphides over a thickness of up to 150 m within pure olivine–sulphide adcumulates with trace chromite. The sulphides take the form of composite pentlandite–pyrrhotite aggregates with minor chalcopyrite and secondary magnetite, developed within the interstitial space between now serpentinized cumulus olivine grains up to 2 cm in size. Nickel tenors (i.e. Ni content of 100% sulphide) range from 12 to 20%, with up to 2 ppm each of Pt and Pd (Barnes *et al.*, 2011).

Goliath and Six Mile

The Goliath and Six Mile deposits (Grguric *et al.*, 2006) occur within the Yakabindie camp, about 20 km south of Mount Keith, and have essentially similar geology and host-rocks.

The Dumont deposit, within the eastern Abitibi greenstone belt in Quebec, Canada, is also hosted by nearly pure adcumulate dunites of komatiitic affinity, and is characterized by distinct internal layering defined mainly by the abundance of sulphide and olivine grain size (Duke, 1986).

Kevitsa

The Kevitsa deposit (~400 million tonnes at 0·29% Ni) is a large body of low-grade disseminated Ni–Cu–PGE sulphide ore with widely variable tenor, hosted within a dominantly pyroxenite, complex layered intrusive body within the central Lapland greenstone belt in northern Finland (Mutanen, 1997; Mutanen & Huhma, 2001; Yang *et al.*, 2013). Disseminated ores are hosted within mesocumulate wehrlites and olivine clinopyroxenites.

Kharealakh

The Kharealakh intrusion at Talnakh, Siberia, hosts several of the major ore deposits of the super-giant Noril'sk–Talnakh camp. Globular and blebby disseminated ores form a high proportion of the lower, olivine-bearing portion of a sill, and are developed within a sequence of cumulate-textured olivine gabbros and gabbros (Czamanske *et al.*, 1995; Lightfoot & Zotov, 2014).

Black Swan

The Black Swan deposit is an ~10 Mt body of disseminated ore hosted within coarse-grained olivine orthocumulates of komatiitic affinity in the Kalgoorlie Terrane of the east Yilgarn Craton about 70 km NE of Kalgoorlie (Dowling *et al.*, 2004; Barnes *et al.*, 2009b).

Marriotts

Marriotts is a small blebby sulphide-dominated disseminated deposit associated with komatiitic olivine orthocumulates 250 km NW of Kalgoorlie.

Expo–Ungava

Expo–Ungava is one of a series of deposits comprising disseminated, matrix and breccia-textured massive ores within ultramafic dykes of komatiitic basalt parentage within the 1·88 Ga Cape Smith Belt of northern Quebec (Mungall, 2007).

APPENDIX B: MEASUREMENTS OF DROPLET SIZES USING MEDICAL X-RAY COMPUTED TOMOGRAPHY

The medical X-ray computed tomography system used for this study is a SOMATON Definition AS Medical CT Scanner. This instrument is composed of a rotating X-ray source producing a fan-shaped X-ray beam, along with a rotating set of X-ray detectors (Multislice UFC™ detectors), and a 100 kW generator. The X-ray source is fitted with an STRATON MX P High Performance CT-X-ray tube, with intensity and voltage ranging from 20 to 800 mA and from 70 to 140 kV, allowing the X-rays to be transmitted through dense and complex material such as disseminated to blebby magmatic nickel sulphides. Detectors measure the absorption of the X-rays (or attenuation), which depends on the atomic number and the density of the material, as well as the spectral characteristics of the X-ray source. However, most samples imaged in this study are heterogeneous, and each pixel will be a record of the total attenuation along the X-ray path. Reconstruction to produce the tomographic dataset was carried out in the Syngo® acquisition workplace.

After reconstruction the dataset represents a regular volumetric grid in which each voxel has a unique greyscale value. This grid was then processed and analysed with AvizoFire® (Visualization Science Group); visualization and quantification was carried out on high-end desktop computers with 32 cores and 192 Gb RAM provided by iVEC at the Australian Resource Research Centre (Perth, Australia). Digital filters were applied to enhance and clean up the images (generally a non-local mean filter was applied), and a segmentation process was carried out, attributing a range of greyscale values to a given phase. Two main phases were chosen for the purpose of this study: silicates and sulphides; quantitative measurements were made to provide information on the shape and size of the sulphide droplets.

APPENDIX C: COMPUTATIONAL FLUID DYNAMICS MODELS

The computational models in Figs 10 and 11 were carried out using Gerris (Popinet, 2003), which solves an octree-based volume of fluid discretization of the Navier–Stokes equations, including surface tension effects, which are present in these simulations. The properties of the sulphide and host magma were determined from the properties listed in Table 1 and non-dimensionalized appropriately.

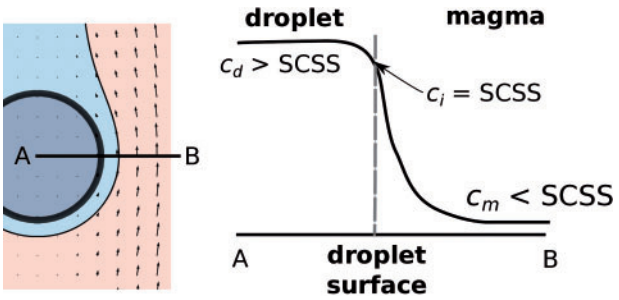

Fig. D1 Schematic illustration of a dissolving droplet, showing the locations of the compositional variables and the chemical gradient across the droplet surface.

1. The laminar break-up simulation in Fig. 10 was formulated using the 'blinking vortex' flow of Aref (1984). In this model two vortices blink on and off on opposite sides of a circular domain, driving the stretching and folding seen in the simulation.
2. The turbulent flow was generated by starting with the Arnold–Beltrami–Childress (ABC) flow (Arnold, 1965; Dombre *et al.*, 1986), and adding energy to the flow until it makes the transition to a fully developed turbulent vortex field (Fuster, 2013). Once the vortex field had stabilized, the sulphide droplet was added, leading to the break-up process illustrated in Fig. 11.

All other simulations used to generate Figs 5–9 were implemented in Python. The code used to generate these simulations is available from the first author on request.

APPENDIX D: DROPLET DISSOLUTION MODEL

The theory for the droplet dissolution model roughly follows Kerr (1994); however, we include it here for completeness using our notation. At the droplet surface the compositional flux out of the droplet is determined by the interfacial gradient and the diffusivity $\kappa_{\mathrm{FeS,m}}$ of FeS in the magma

$$f = \kappa_{\mathrm{FeS,m}} \left(\frac{\mathrm{d}c_{\mathrm{FeS}}}{\mathrm{d}r} \right)_{r=a}. \tag{22}$$

Separating the boundary of the droplet from the magma is a corresponding compositional boundary layer, whose thickness is given by

$$\delta = \kappa_{\mathrm{FeS,m}} \left(\frac{c_{\mathrm{m}} - c_{\mathrm{i}}}{f} \right) \tag{23}$$

where c_{m} is the concentration of the sulphur in the magma far from the droplet surface, and c_{i} is the concentration at the droplet interface (shown in Fig. D1). If there is no significant volume change associated with the phase change across the droplet boundary, then f is related to the velocity of dissolution by

$$\frac{\mathrm{d}a}{\mathrm{d}t} = \frac{f}{c_{\mathrm{i}} - c_{\mathrm{d}}} \tag{24}$$

where c_{d} is the concentration of sulphide in the droplet, which we will assume is $\sim$1. By combining the two expressions to remove f we can obtain a relationship between the boundary layer thickness and the dissolution velocity.

The compositional flux out of the droplet can be rewritten in terms of the Sherwood number Sh. In terms of the compositional boundary layer, we have $\delta = a/\mathrm{Sh}(a)$. Then, using the expressions for dissolution velocity and boundary layer above, we see that

$$\frac{\mathrm{d}a}{\mathrm{d}t} = \kappa_{\mathrm{s,m}} \left(\frac{c_{\mathrm{m}} - c_{\mathrm{i}}}{c_{\mathrm{i}} - c_{\mathrm{d}}} \right) \frac{\mathrm{Sh}(a)}{a}. \tag{25}$$

To close our model we need to specify c_{i}, the concentration of the sulphide at the surface of the droplet. Because Sc $\gg$ Pr, the droplet reaches thermal equilibrium with the magma much faster than chemical equilibrium. This means that the surface of a droplet will always be in thermodynamic equilibrium with the melt immediately adjacent to it. Hence the sulphur concentration immediately beside the interface of a droplet will always be given by the local value of the SCSS; that is, $c_{\mathrm{i}} \approx \mathrm{SCSS}(P, T)$. Hence,

$$\frac{\mathrm{d}a}{\mathrm{d}t} = \kappa_{\mathrm{s,m}} \left(\frac{c_{\mathrm{m}} - \mathrm{SCSS}}{\mathrm{SCSS} - c_{\mathrm{d}}} \right) \frac{\mathrm{Sh}(a)}{a} \tag{26}$$

as used in the main body of the text.